AIAA JOURNAL
Vol. 49, No. 3, March 2011

Adaptive Control of Nonlinear Free Vibration of Shallow Shell Using Piezoelectric Actuators

Minseock Park*
Old Dominion University, Norfolk, Virginia 23529
Adam Przekop†
Analytical Services and Materials, Inc., Hampton, Virginia 23666
Thongchai Phairoh‡
Virginia State University, Petersburg, Virginia 23806
and
Jen-Kuang Huang§ and Chuh Mei¶
Old Dominion University, Norfolk, Virginia 23529

DOI: 10.2514/1.38520

A coupled structural-electrical nonlinear modal finite-element multiple-mode formulation for laminated composite shallow shells with embedded piezoelectric sensors and actuators is presented for the suppression of large-amplitude undamped free vibrations. Composite shells exhibiting both softening and hardening behavior are investigated. The linear quadratic regulator combined with an extended Kalman filter is employed as an active controller for the suppression of nonlinear free vibrations. However, when the frequency of limit-cycle oscillations is suddenly changed from the softening to the hardening response characteristics or vice versa, active controller has difficulties to adjust the control parameters to cope with the changed structural response. To mitigate this issue, the currently developed controller is adaptively designed using the system identification which has the ability to identify the frequency of limit-cycle oscillations. It is shown that the adaptive controller constructed of the linear quadratic regulator and extended Kalman filter with system identification is suitable for suppression of the sudden change of shallow-shell response characteristics. The norm of optimal feedback control gain method for actuators and the norm of Kalman filter estimator gain method for sensors are employed to determine their optimal locations, respectively. Two different self-sensing actuator types, PZT5A and macrofiber composite, are used and their control performance for the suppression of the oscillations is compared. The numerical results illustrate that the adaptive controller can successfully suppress the nonlinear free vibrations, even with unknown sudden changes in the multimode response characteristic.

Nomenclature

$\bar{\boldsymbol{A}}$, $\boldsymbol{B}$, $\boldsymbol{C}$, $\boldsymbol{D}$	=	system state-space matrices
$[A]$, $[B]$, $[D]$, $[A_s]$	=	in-plane, coupled in-plane bending, bending, and shear material stiffness matrices
h	=	panel thickness
$[K_{b\phi}]$	=	coupled bending and electrical stiffness matrix
$[K_L]$, $[\bar{K}_L]$	=	linear and linear modal stiffness matrices
$[K_q]$, $[K_{qq}]$	=	modal first-order and second-order nonlinear stiffness matrices
$[K_1]$, $[K_2]$	=	first-order and second-order nonlinear stiffness matrices
$[M]$, $[\bar{M}]$	=	mass and modal mass matrices
$\boldsymbol{Q}$	=	symmetric positive semidefinite state weighting matrix
$\boldsymbol{Q_e}$, $\boldsymbol{R_e}$	=	covariance matrices
$\{q\}$	=	generalized modal coordinate vector
$\{q^s\}$	=	sensor charge output vector
R	=	shell radius
$\boldsymbol{R}$	=	symmetric positive definite control effort weighting matrix
$\boldsymbol{U}$	=	control input
$\{U\}$, $\{V\}$	=	in-plane displacements along x and y axes
V_i	=	constant electrical voltage over the i-th piezoelectric layer
$\{W\}$	=	system node degrees-of-freedom vector
$\boldsymbol{X}$, $\hat{\boldsymbol{X}}$	=	actual and estimated state vectors
$\boldsymbol{Y}$, $\hat{\boldsymbol{Y}}$	=	sensor output and estimated output vectors
$\{\gamma_s\}$	=	shear strain
$\{\varepsilon^o\}$	=	in-plane strain vector
$\{\kappa\}$	=	bending curvature
ρ	=	mass density
$[\phi]$	=	eigenvector matrix
ω	=	frequency

Subscripts

b	=	bending
L	=	linear
max	=	maximum
min	=	minimum
N_b	=	referring to $[B]\{\kappa\}$
N_m	=	referring to $[A]\{\varepsilon_m^o\}$
NL	=	nonlinear
np	=	total number of piezoelectric layers per element

Received 27 May 2008; revision received 30 August 2010; accepted for publication 25 September 2010.

*Research Assistant, Department of Mechanical and Aerospace Engineering; presently Aircraft Development Team, MUAV Development Center, Korean Air, 461-1, Jeonmin-dong, Yusung-Gu Daejeon 305-811, Republic of Korea; mseockpark@koreanair.com. Student Member AIAA.

†Senior Structural Engineer, c/o NASA Langley Research Center, Mail Stop 463; Adam.Przekop@nasa.gov. Senior Member AIAA.

‡Assistant Professor, Department of Engineering and Technology, 1 Hayden Drive; tphairoh@vsu.edu.

§Professor and Chair, Department of Mechanical and Aerospace Engineering, 238 Kaufman Hall; jhuang@odu.edu. Member AIAA.

¶Eminent Scholar Emeritus and Professor Emeritus, Department of Mechanical and Aerospace Engineering, 238 Kaufman Hall; cmei@odu.edu. Associate Fellow AIAA.

R = radius
r = mode number
s = shear
x = x axis
y = y axis

I. Introduction

SHALLOW shells are common structural components in aerospace and other engineering applications. Despite the fact that most of the practical problems involve a forced response prediction, the free-vibration studies of shallow shells lend a valuable insight into their structural dynamic response prediction.

Liew et al. [1] reviewed the vibration of shallow shells, and various theories have been described. Marguerre curved plate theory was used by Cummings [2] to study large-amplitude vibration of a freely supported cylindrical shell segment. Donnell's shell theory was applied by Hui [3] for simply supported cylindrical panels with geometric imperfections. Raouf and Palazotto [4] used the Donnel-Mushtari-Vlasov shell theory to model curved orthotropic cylindrical panel using the Galerkin procedure and perturbation method. Abe et al. [5] studied nonlinear vibration of clamped laminated shallow shells by considering the first two modes (first symmetrical and first antisymmetrical). They investigated the influence of the first mode on nonlinear vibration of the second mode. Pillai and Rao [6], and Bhimaraddi [7] were concerned with the softening effect in flat plates due to antisymmetrical lamination. Interestingly, in the curved panel the softening effect can be either magnified or suppressed by the stacking sequence of the symmetric or antisymmetrical lamination. Classical analysis have neglected the in-plane inertia terms due to mathematical difficulties. Shi et al. [8] studied the coupled linear bending-in-plane modes to obtain the nonlinear general Duffing equations. Przekop et al. [9] investigated the differences in a shallow-shell response prediction when uncoupled versus coupled linear bending and in-plane modes are used. They also concluded that the in-plane inertia can be neglected in the nonlinear response simulation of shallow shells.

To control the global dynamic behavior of the flexible structures, the active modal controller methodologies have been developed. Inman [10] established the modal control techniques to manage the problems of control spillover which is caused by the structural flexibility. He pointed out the application of numerous sensors and actuators providing an effective and simple solution to problems associated with control of flexible structures. Zhang [11] used the natural second-order form of the equations of motion to design the optimal vibration control. The optimal control feedback matrices were obtained by solving a set of linear differential equations. Xie et al. [12] employed H-infinite control method to suppress the low-frequency modal vibration of the thin plate covered with a controllable constrained damping layer. They considered disturbance/output characteristic of the structure in robust control design. Abdel-Motagaly and Mei [13] investigated the application of the adaptive feedback linearization controller to suppress the free vibrations of a simply supported beam. De Abreu and Ribeiro [14] proposed an online self-organizing fuzzy logic controller to control of vibrations in flexible structures. Hossain et al. [15] studied genetic algorithm and adaptive neurofuzzy inference system to develop a control mechanism for suppression of transverse vibration motion of flexible beam. Li et al. [16] showed the application of adaptive control method for nonlinear free vibrations of the flat plate using piezoelectric actuators.

The free response structural analysis carries its inherent complexities. In particular, obtaining the exact initial condition for the steady periodic multimode solution is a challenge and, therefore, most published studies are limited to a single-mode approach. In the current paper an improved multiple-mode approach is offered and since the judicious initial conditions are necessary to compute multimode solution, an iterative procedure is introduced. A shallow-shell finite element (FE) with the improved shear correction factor is used in the formulation. Composite curved panels with different lamination stacking sequences are employed to simulate the hardening- and softening-dominant vibrations. The von Karman nonlinear strain-displacement relations, classical laminated composite plate theory, the first-order shear deformation theory, and linear piezoelectricity constitutive relations are employed in the coupled electrical-structural FE formulation of nonlinear free-vibration in the physical coordinates. The system equations of motion are then transformed into a reduced-size set of equations in the modal coordinates. As for the self-sensing actuators, PZT5A [17] and MFC [18] piezoelectric smart materials are applied to composite curved panels. The norms of feedback control gain [19] (NFCG) and the norms of Kalman filter estimation gain [20] (NKFEG) methods guide the favorable location of self-sensing actuators. The linear quadratic regulator (LQR) combined with the extended Kalman filter (EKF) are designed to suppress the vibration amplitudes. System ID permits identification of the nonlinear frequency of the system to facilitate the control of the qualitatively changing structural response characteristic. The controller is optimized to suppress corresponding dynamic motions. To the authors' knowledge, it is the first study in designing the multiple-mode adaptive controller for a shallow-shell structure with the objective of suppressing both hard- and soft-spring behaviors.

II. Finite-Element Formulation

A. System Equations of Motion in Physical Degrees of Freedom

A fully coupled structural-electric FE formulation is developed to incorporate isotropic (PZT5A) and anisotropic (MFC) piezoelectric smart materials in shell structures. The triangular Mindlin [21,22] (MIN3) FE with the improved shear correction factor and additionally enhanced with an additional electric potential degrees of freedom (DOF) to model the embedded piezoelectric actuators and sensors is developed. The electric DOF is assumed constant over the each piezoelectric layer. The first-order shear deformation theory for a curved shallow shell is presented considering the von Karman large deflection. The large deflection strain-displacement relations of the Mindlin first-order shear deformation theory are given by [21] as

$$\{\varepsilon\} = \{\varepsilon^o\} + z\{\kappa\} \tag{1}$$

where

$$\{\varepsilon^o\} = \{\varepsilon^o_m\} + \{\varepsilon^o_b\} + \{\varepsilon^o_R\} = \begin{Bmatrix} u_{,x} \\ v_{,y} \\ u_{,y} + v_{,x} \end{Bmatrix} + \frac{1}{2}\begin{Bmatrix} w^2_{,x} \\ w^2_{,x} \\ 2w_{,x}w_{,y} \end{Bmatrix} + \begin{Bmatrix} w/R_x \\ w/R_y \\ 0 \end{Bmatrix}$$

$$\{\kappa\} = \begin{Bmatrix} \psi_{y,x} \\ \psi_{x,y} \\ \psi_{x,x} + \psi_{y,y} \end{Bmatrix}, \qquad \{\gamma_s\} = \begin{Bmatrix} w_{,y} \\ w_{,x} \end{Bmatrix} + \begin{Bmatrix} \psi_x \\ \psi_y \end{Bmatrix} - \begin{Bmatrix} u/R_x \\ v/R_y \end{Bmatrix}$$

The electrical field-potential relations for the piezoelectric layers are comparable to mechanical strain-displacement relations. The electrical field can be written in terms of the electrical DOF defined as

$$\begin{Bmatrix} E_1 \\ \vdots \\ E_{\text{np}} \end{Bmatrix} = -[B_\phi]\{w_\phi\} = -\begin{bmatrix} \frac{1}{h_1} & \cdots & 0 \\ \vdots & \ddots & \vdots \\ 0 & \cdots & \frac{1}{h_{\text{np}}} \end{bmatrix}\begin{Bmatrix} V_1 \\ \vdots \\ V_{\text{np}} \end{Bmatrix} \tag{2}$$

where h_i is the thickness of the i-th piezoelectric layer, and the polarization of isotropic piezoelectric materials is generated in the 3-direction, and that of anisotropic materials is in the 1-direction. The constitutive equations (stress-strain relations) of the k-th layer of a fiber reinforced laminated composite curved panel with embedded piezoelectric layers are introduced next. Considering the k-th piezoceramic layer the coupled stress resultants of force and moment per unit length are expressed as

$$\begin{Bmatrix} N \\ M \\ Q \end{Bmatrix} = \begin{bmatrix} A & B & 0 \\ B & D & 0 \\ 0 & 0 & A_s \end{bmatrix} \begin{Bmatrix} \varepsilon^o \\ \kappa \\ \gamma_s \end{Bmatrix} - \begin{Bmatrix} N_\phi \\ M_\phi \\ 0 \end{Bmatrix} \tag{3}$$

where

$$(\{N_\phi\}, \{M_\phi\}) = \int_{-h/2}^{h/2} [\bar{Q}]_k \{d\}_k E_{ik}(1, z)\, \mathrm{d}z \tag{4}$$

$$([A], [B], [D]) = \int_{-h/2}^{h/2} [\bar{Q}]_k (1, z, z^2)\, \mathrm{d}z \tag{5}$$

The piezoelectric charge constant in the principal axes is $\{d\}_k^T = [\, d_{31} \quad d_{32} \quad 0\,]$, with $d_{32} = d_{31}$ and $i = 3$ for PZT5A actuators, and $\{d\}_k^T = [\, d_{11} \quad d_{12} \quad 0\,]$ and $i = 1$ for MFC actuators [18,19], where d_{11} of MFC has the advantage of being twice as large as the value of d_{31} of PZT5A. As for the application of effective actuator motion, bending moment $\{M_\phi\}$ is applied by setting the equal amplitude but opposite sign of voltages on the top and bottom of piezoelectric layers for both PZT5A and MFC actuators. The in-plane piezoelectric actuation force $\{N_\phi\}$ is negligible for suppression of the limit-cycle oscillations (LCO) of the curved panel [23].

FE equations of motion for the laminated composite shell with fully coupled electrical-structural properties are obtained based on the Hamilton's principle. Following standard assembly procedures of element matrices the global equations of motion can be expressed [24] as

Actuator equation:

$$\begin{bmatrix} [M_b] & 0 \\ 0 & [M_m] \end{bmatrix} \begin{Bmatrix} \ddot{W}_b \\ \ddot{W}_m \end{Bmatrix} + \left(\begin{bmatrix} [K_b] + [K_b^s] + [K_b^R] & [K_{bm}] + [K_{bm}^{sR}] + [K_{bm}^R] \\ [K_{mb}] + [K_{mb}^{sR}] + [K_{mb}^R] & [K_m] + [K_m^{sR}] \end{bmatrix} + \begin{bmatrix} [K1_b] + [K1_b^{N_b}] + [K1_b^{Nm}] + [K1_b^R] + [K1_b^{N_{CR}}] & [K1_{bm}] \\ [K1_{mb}] & 0 \end{bmatrix} + \begin{bmatrix} [K2_b] & 0 \\ 0 & 0 \end{bmatrix} \right) \begin{Bmatrix} W_b \\ W_m \end{Bmatrix} = -\begin{bmatrix} [K_{b\phi}] \\ 0 \end{bmatrix} \{W_\phi\} \tag{7}$$

Sensor equation:

$$\{q^s\} = -[K_{\phi b}]\{W_b\} \tag{8}$$

B. Modal Formulation

The nonlinear system equation of motion, Eq. (7), can be very large and therefore its direct numerical integration can become computationally intensive. To gain computational efficiency a modal reduction process can be performed. The nonlinear stiffness matrices $[K1]$ and $[K2]$ rely on the unknown structural displacements $\{W\} = [\{W_b\}, \{W_m\}]$, where $\{W_b\}^T = [\{W_t\}^T, \{\Psi_x\}^T, \{\Psi_y\}^T]$ and $\{W_m\}^T = [\{U\}^T, \{V\}^T]$, what consequently requires them to be updated repeatedly throughout the time integration process. High frequencies and small amplitudes of the in-plane motion allow an approximation where the in-plane inertial term is neglected in Eq. (7). Thus, the in-plane displacement $\{W_m\}$ can be expressed with respect to the transverse displacement vector $\{W_b\}$ as

$$\{W_m\} = -([K_m] + [K_m^{sR}])^{-1}([K_{mb}] + [K_{mb}^R] + [K_{mb}^{sR}] + [K1_{mb}])\{W_b\} \tag{9}$$

Substituting Eq. (9) into Eq. (7), equation of motion is represented as a function of bending displacement only, i.e.,

$$[M_b]\{\ddot{W}_b\} + ([K_b] + [K_b^s] + [K_b^R] + [K1_b] + [K1_b^{N_b}] + [K1_b^{N_m}] + [K1_b^R] + [K1_b^{N_{CR}}] + [K2_b] - ([K_{bm}] + [K_{bm}^{sR}] + [K_{bm}^R] + [K1_{bm}])([K_m] + [K_m^{sR}])^{-1} \times ([K_{mb}] + [K_{mb}^R] + [K_{mb}^{sR}] + [K1_{mb}]))\{W_b\} = -[K_{b\phi}]\{W_\phi\} \tag{10}$$

The expansion of Eq. (10) results in 16 new linear terms, six first-order nonlinear terms and 1 s-order nonlinear [9]. Moreover, the first-order nonlinear term $[K1_b^{N_m}]$ is a function of the in-plane displacement $\{W_m\}$ itself which leads to a further expansion. The physical bending displacement component $\{W_b\}$ can be expressed as a summation of the modal bending displacement bases $\{\phi_b\}$ as

$$\{W_b\} = \sum_{r=1}^{n} q_r(t)\{\phi_b\}^{(r)} = [\phi_b]\{q\} \tag{11}$$

The number of needed linear modes, n, is much smaller than the number of physical DOF in bending $\{W_b\}$. Mode-shape $\{\phi_b\}^{(r)}$ is developed from the linear eigen-problem defined as

$$\omega_r^2[M_b]\{\phi_b\}^{(r)} = [K_{Lb}]\{\phi_b\}^{(r)} \tag{12}$$

where $[K_{Lb}]$ consists of all the linear terms in Eq. (10). The normal mode $\{\phi_r\}$ is normalized with the absolute maximum component to unity. Therefore, the modal mass matrix and the modal linear stiffness matrix become

$$[\bar{M}_b] = [\phi_b]^T[M_b][\phi_b] \tag{13}$$

$$[\bar{K}_{Lb}] = [\phi_b]^T[K_{Lb}][\phi_b] \tag{14}$$

The nonlinear stiffness matrices in the modal coordinates can be written as

$$[K_{qb}] = [\phi_b]^T \sum_{r=1}^{n} q_r(t)[K1_b(\phi)]^{(r)}[\phi_b] \tag{15}$$

$$[K_{qqb}] = [\phi_b]^T \sum_{r=1}^{n}\sum_{s=1}^{n} q_r(t)q_s(t)[K2_b(\phi)]^{(rs)}[\phi_b] \tag{16}$$

Actuator equation, Eq. (10), in the modal bending coordinates can be expressed as

$$[\bar{M}_b]\{\ddot{q}\} + ([\bar{K}_{Lb}] + [K_{qb}] + [K_{qqb}])\{q\} = -[\bar{K}_{b\phi}]\{W_\phi\} \tag{17}$$

Sensor equation, Eq. (8), in the modal bending coordinates can be expressed as

$$\{q^s\} = -[\bar{K}_{\phi b}]\{q\} \tag{18}$$

where the expressions for $[K_{Lb}]$, $[K_{qb}]$ and $[K_{qqb}]$ are derived in [9]. For the multimode solutions, the dominant modes to be included in the modal transformation are selected based on the modal participation for the converged LCO solution. The participation of the r-th mode can be expressed as

$$\text{Participation of the } r\text{-th mode} = \frac{\max|q_r(t)|}{\sum_{s=1}^{n}\max|q_s(t)|} \tag{19}$$

III. Adaptive Controller Methodology

A. Linear Quadratic Regulator/Extended Kalman Filter

In developing the control system, LQR along with EKF is provided based on the closed-loop design method. To get all state variables measured, the estimator must be incorporated to obtain the unmeasurable state variables. The mathematical model in modal coordinates from Eqs. (17) and (18) is used to analyze a control system performance. It is essential to represent the system equations into the standard state-space form written as

$$\dot{\boldsymbol{X}} = \bar{\boldsymbol{A}}\boldsymbol{X} + \boldsymbol{B}\boldsymbol{U} \qquad \boldsymbol{Y} = \boldsymbol{C}\boldsymbol{X} + \boldsymbol{D}\boldsymbol{U} \tag{20}$$

where

$$\boldsymbol{X} = \begin{Bmatrix} q \\ \dot{q} \end{Bmatrix}, \qquad \boldsymbol{U} = \{W_\phi\}, \qquad \boldsymbol{Y} = \{q^s\} \tag{21}$$

$$\bar{\boldsymbol{A}} = \boldsymbol{A} + \boldsymbol{A_q} = \begin{bmatrix} 0 & \boldsymbol{I} \\ -[\bar{M}_b]^{-1}[\bar{K}_{Lb}] & 0 \end{bmatrix} + \begin{bmatrix} 0 & 0 \\ -[\bar{M}_b]^{-1}([\bar{K}_{qb}] + [\bar{K}_{qqb}]) & 0 \end{bmatrix}$$
$$\boldsymbol{B} = \begin{bmatrix} 0 \\ -[\bar{M}_b]^{-1}[\bar{K}_{b\phi}] \end{bmatrix}, \qquad \boldsymbol{C} = [\,-[\bar{K}_{\phi b}] \quad 0\,], \qquad \boldsymbol{D} = 0 \tag{22}$$

The total system state matrix $\bar{\boldsymbol{A}}$ is separated into the linear part $\boldsymbol{A}$ and nonlinear part $\boldsymbol{A_q}$. First step of contriving the controller is to compute the state feedback control gain matrix of LQR. Note, that only the first term $\boldsymbol{A}$ is considered in Eq. (22) in applying the optimal law in Eq. (24). The estimated states $\hat{\boldsymbol{X}}$ will be observed from EKF system:

$$\boldsymbol{U} = -\boldsymbol{K}\hat{\boldsymbol{X}} \tag{23}$$

The feedback gain $\boldsymbol{K}$ matrix of the LQR controller can be optimized by minimizing a quadratic performance index $\boldsymbol{J}$:

$$\boldsymbol{J} = \int_0^\infty [\boldsymbol{X}^T\boldsymbol{Q}\boldsymbol{X} + \boldsymbol{U}^T\boldsymbol{R}\boldsymbol{U}]\,\mathrm{d}t \tag{24}$$

$$\boldsymbol{K} = \boldsymbol{R}^{-1}\boldsymbol{B}^T\boldsymbol{P} \tag{25}$$

The matrices $\boldsymbol{Q}$ and $\boldsymbol{R}$ are selected to satisfy the condition of the positive definite symmetric matrix. The solution of the algebraic Riccati equation determines the matrix $\boldsymbol{P}$ given by

$$\boldsymbol{A}^T\boldsymbol{P} + \boldsymbol{P}\boldsymbol{A} - \boldsymbol{P}\boldsymbol{B}\boldsymbol{R}^{-1}\boldsymbol{B}^T\boldsymbol{P} + \boldsymbol{Q} = 0 \tag{26}$$

The estimated state variables are returned through the EKF. Those variables are used in output feedback by comparing the difference between real and estimated measurement information. The second term $\boldsymbol{A_q}$ in Eq. (22) is considered to compensate the nonlinear part of the dynamic response. The nonlinear state estimation and measurement are expressed as

$$\dot{\hat{\boldsymbol{X}}} = \bar{\boldsymbol{A}}(\hat{\boldsymbol{X}}, t)\hat{\boldsymbol{X}} + \boldsymbol{B}\boldsymbol{U} + \boldsymbol{K_e}(t)(\boldsymbol{Y} - \boldsymbol{C}\hat{\boldsymbol{X}}), \qquad \hat{\boldsymbol{Y}} = \boldsymbol{C}\hat{\boldsymbol{X}} \tag{27}$$

Taylor's series are applied to pursue the first-order linear approximation coefficients to cope with the nonlinear matrices as follows:

$$\boldsymbol{F}(t) \approx \left.\frac{\partial \boldsymbol{f}(\boldsymbol{X}, t)}{\partial \boldsymbol{X}}\right|_{X=\hat{X}(t)} = \begin{bmatrix} \frac{\partial f_1}{\partial X_1} & \frac{\partial f_1}{\partial X_2} & \frac{\partial f_1}{\partial X_3} & \cdots & \frac{\partial f_1}{\partial X_n} \\ \frac{\partial f_2}{\partial X_1} & \frac{\partial f_2}{\partial X_2} & \frac{\partial f_2}{\partial X_3} & \cdots & \frac{\partial f_2}{\partial X_n} \\ \frac{\partial f_3}{\partial X_1} & \frac{\partial f_3}{\partial X_2} & \frac{\partial f_3}{\partial X_3} & \cdots & \frac{\partial f_1}{\partial X_n} \\ \vdots & \vdots & \vdots & \ddots & \vdots \\ \frac{\partial f_n}{\partial X_1} & \frac{\partial f_n}{\partial X_2} & \frac{\partial f_n}{\partial X_3} & \cdots & \frac{\partial f_n}{\partial X_n} \end{bmatrix}_{X=\hat{X}(t)} \tag{28}$$

where

$$\boldsymbol{f}(\boldsymbol{X}, t) = \dot{\boldsymbol{X}} = \bar{\boldsymbol{A}}(\boldsymbol{X}, t)\boldsymbol{X} + \boldsymbol{B}\boldsymbol{U} \tag{29}$$

$$\boldsymbol{X} = [\boldsymbol{X}_1\boldsymbol{X}_2\boldsymbol{X}_3 \cdots \boldsymbol{X}_n]^T$$
$$\boldsymbol{F}(t) \approx \boldsymbol{A} + \left(\boldsymbol{A_q}(\boldsymbol{X}, t) + \frac{\partial \boldsymbol{A_q}(\boldsymbol{X}, t)}{\partial \boldsymbol{X}}\boldsymbol{X}\right)\Big|_{X=\hat{X}(t)} \tag{30}$$

The differential Riccati equation determines the Kalman optimal filter gain $\boldsymbol{K_e}$. Since the nonlinear term is updated online, the EKF gain is computed at every time interval resulting from

$$\dot{\boldsymbol{P}}_{\boldsymbol{e}}(t) = \boldsymbol{F}(t)\boldsymbol{P_e}(t) + \boldsymbol{P_e}(t)\boldsymbol{F}(t)^T - \boldsymbol{P_e}(t)\boldsymbol{C}^T\boldsymbol{R_e}^{-1}\boldsymbol{C}\boldsymbol{P_e}(t) + \boldsymbol{Q_e} \tag{31}$$

$$\boldsymbol{K}_{\boldsymbol{e}}(t) = \boldsymbol{P_e}(t)\boldsymbol{C}^T\boldsymbol{R_e}^{-1} \tag{32}$$

The optimal location of self-sensing piezoelectric actuators are obtained based on the norms of feedback gain designed for the LQR in Eq. (25) and the norms of feedback gain designed for the EKF in Eq. (32):

$$NFCG = \sqrt{\sum_{j=1}^{2n} \boldsymbol{K}_{ij}^2}, \qquad NKFEG = \sqrt{\sum_{j=1}^{2n} \boldsymbol{K}_{eij}^2} \tag{33}$$

B. System Identification

In 1992, a novel approach has been developed by Chen et al. [25] to integrate system identification and state estimation. Phan et al. [26] derived a versatile approach for system identification: the observer/Kalman filter identification algorithm. This algorithm diminishes the effects of noise on the identified system parameters. It has been proven to be numerically efficient and robust with respect to measurement noise, even in the presence of mild nonlinearities. A number of successful applications of this method have been documented, for instance in the areas of structural mechanics and aerospace engineering [27]. For the adaptive control, system ID is required to identify the frequency of LCO. The frequency detected by system ID is then used for LQR/EKF to suppress vibrations. Since system ID has to be evaluated online, it can be regarded as online identification. Accordingly, the adaptive control is based on an input-output model. In an input-output model, the output variable is described directly in terms of the input variable while the state-space representation describes the relationship in terms of an intermediate variable, the system state. The autoregressive model with exogenous input (ARX), where the system output at the current time step is described as a linear combination of a certain number of past input and output values, is used as the following input-output model:

$$y(k) = \alpha_1 y(k-1) + \alpha_2 y(k-2) + \cdots + \alpha_p y(k-p) + \beta_0 u(k) + \beta_1 u(k-1) + \beta_2 u(k-2) + \cdots + \beta_p u(k-p) \tag{34}$$

Equation (34) has m outputs and r control inputs. Thus, the dimension of output $y(k)$ and input $u(k)$ is $m \times 1$ and $r \times 1$ at time k, respectively. The coefficients α_i and β_i called observer Markov parameters with $i = 1, 2, \ldots, p$ (p is the system order) must be identified during operation. In this study, the system become a second order involving only one output y ($\beta_i = 0$) since the system is periodic with a constant nonlinear frequency. Equation (34) can then be simplified as

$$y(k) = \alpha_1 y(k-1) + \alpha_2 y(k-2) \tag{35}$$

System parameters or Markov parameters α_i and β_i can be found by using the recursive least squares method. Equation (34) can be written in a vector form:

$$y(k) = \bar{Y} v_p(k-1) \tag{36}$$

where

$$\bar{Y} = [\,\alpha_1 \quad \alpha_2 \quad \cdots \quad \alpha_p \quad \beta_0 \quad \beta_1 \quad \beta_2 \quad \cdots \quad \beta_p\,] \tag{37}$$

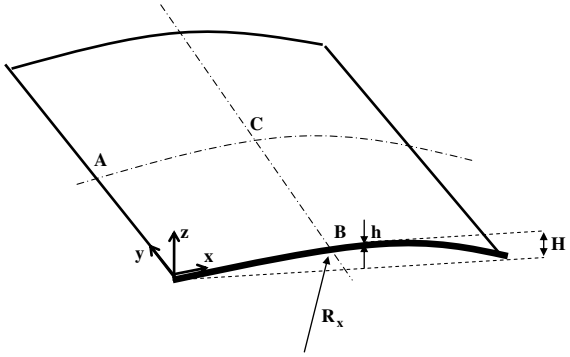

Fig. 1 Cylindrical panel geometry.

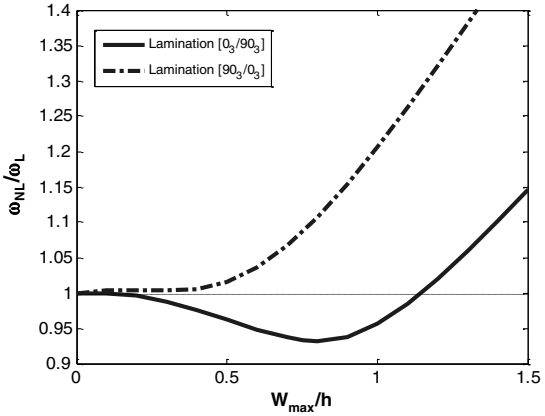

Fig. 2 Lamination stacking sequence influence on the simply supported cylindrical rectangular panel response.

$$v_p(k-1) = \begin{bmatrix} y(k-1) \\ \vdots \\ y(k-p) \\ u(k) \\ \vdots \\ u(k-p) \end{bmatrix} \tag{38}$$

For different values of k, Eq. (36) can be rewritten as

$$y = \bar{Y} V_p \tag{39}$$

where

$$\begin{aligned} y &= [\, y(k) \quad y(k+1) \quad \cdots \quad y(k+N-p-1)\,] \\ V_p &= [\, v_p(k-1) \quad v_p(k) \quad \cdots \quad v_p(k+N-p-2)\,] \\ &\qquad (k = p+1, p+2, \ldots) \end{aligned} \tag{40}$$

The integer N is the number of samples processed in the system ID. The system parameters, at time $(k+N-p-2)+1$, can be identified by using the least squares method:

$$\hat{\bar{Y}}_p = y V_p^T [V_p V_p^T]^+ \tag{41}$$

where the superscript symbol "+" represents pseudo inverse of matrix.

For the system under consideration, Eq. (39) can be simplified by substituting Eq. (35) to yield

$$\begin{aligned} y(k) &= \bar{Y} v_p(k-1) \\ &= [\, \alpha_1 \quad \alpha_2\,] \begin{bmatrix} y(k-1) \\ y(k-2) \end{bmatrix} \end{aligned} \tag{42}$$

For a different value of k, Eq. (42) can be expressed as

$$\begin{aligned} &[\, y(k) \quad y(k+1) \quad \cdots \quad y(k+N-p-1)\,] \\ &= [\, \bar{Y} v_p(k-1) \quad \bar{Y} v_p(k) \quad \cdots \quad \bar{Y} v_p(k+N-p-2)\,] \\ &= \bar{Y} [\, v_p(k-1) \quad v_p(k) \quad \cdots \quad v_p(k+N-p-2)\,] \\ &= [\, \alpha_1 \quad \alpha_2\,] \begin{bmatrix} y(k-1) & y(k) & \cdots & y(k+N-p-2) \\ y(k-2) & y(k-1) & \cdots & y(k+N-p-3) \end{bmatrix} \end{aligned} \tag{43}$$

Using Markov parameters obtained from Eq. (43), the corresponding characteristic equation of LCO can be expressed as

$$z^2 - \alpha_1 z - \alpha_2 = 0 \tag{44}$$

This characteristic equation can be used to identify the LCO frequency. After determining the roots of the characteristic equation, the free-vibration natural frequency is calculated by using the relationship between Z-domain and S-domain for the poles:

$$z = e^{sT} \tag{45}$$

where T is the sampling time. One of the roots of the characteristic equation is the discrete system pole:

$$z = z_0 + j z_1 \tag{46}$$

It can be represented as

$$z = \sqrt{(z_0^2 + z_1^2)}(z_0' + j z_1') = e^{s_1 T} e^{j s_2 T} \tag{47}$$

with

$$\sqrt{(z_0^2 + z_1^2)} = e^{s_1 T} \tag{48}$$

and

$$(z_0' + j z_1') = e^{j s_2 T} \tag{49}$$

where

$$z_0' = \frac{z_0}{\sqrt{(z_0^2 + z_1^2)}}, \qquad z_1' = \frac{z_1}{\sqrt{(z_0^2 + z_1^2)}} \tag{50}$$

For the discrete pole location z, one can calculate S_1 and S_2 and obtain the system pole $S_1 + jS_2$ in the S-domain. The system frequency can be calculated as

Table 1 Natural frequencies for a graphite-epoxy rectangular cylindrical simply supported panel without and with actuators embedded at the top and the bottom layers

	Frequency, Hz			
Material, $[0_3/90_3]$ lamination	Mode (1,1)	Mode (3,1)	Mode (1,3)	Mode (3,3)
Graphite-epoxy	261.32	331.74	536.52	657.00
Graphite-epoxy with embedded MFC (see Appendix B)	232.64	297.68	487.79	652.45
Graphite-epoxy with embedded PZT5A (see Appendix B)	243.89	306.15	535.64	665.52

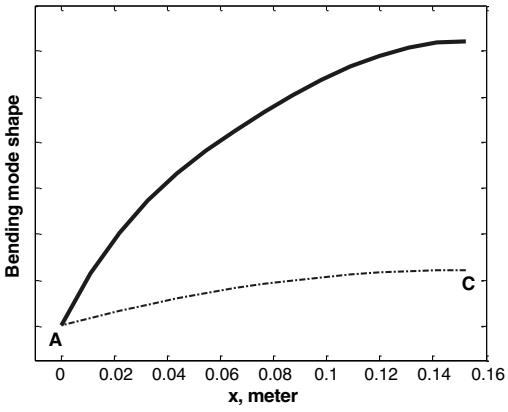

a) Bending mode (1,1) along A-C

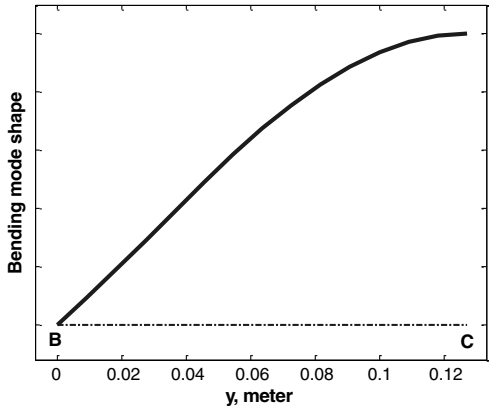

b) Bending mode (1,1) along B-C

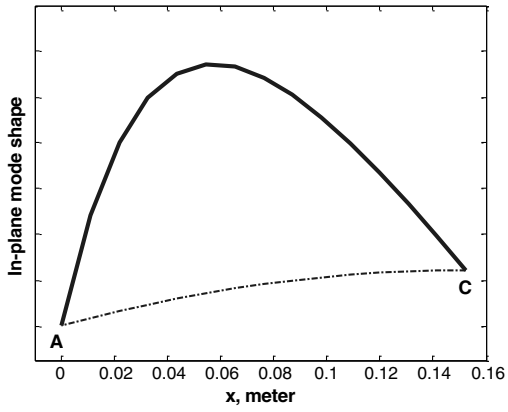

c) In-plane mode (1,1) along A-C

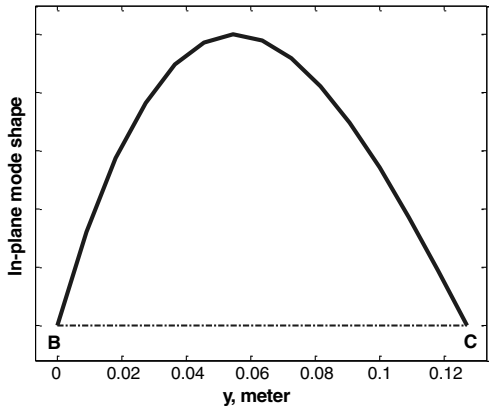

d) In-plane mode (1,1) along B-C

Fig. 3 Bending and in-plane mode shapes of mode (1,1) for a quarter of the simply supported $[0_3/90_3]$ cylindrical panel along A–C and B–C in Fig. 1.

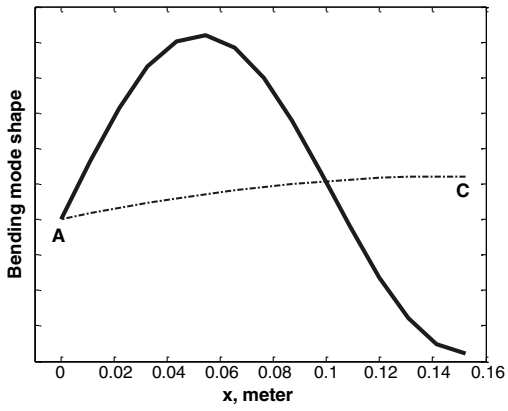

a) Bending mode (3,1) along A-C

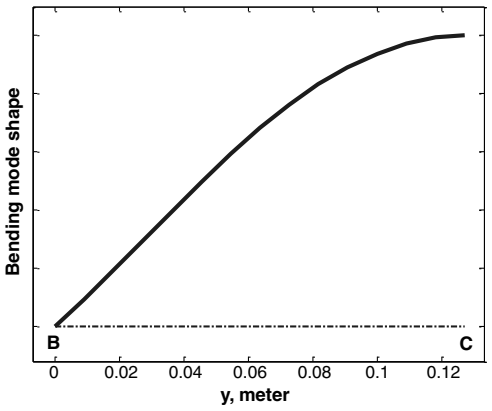

b) Bending mode (3,1) along B-C

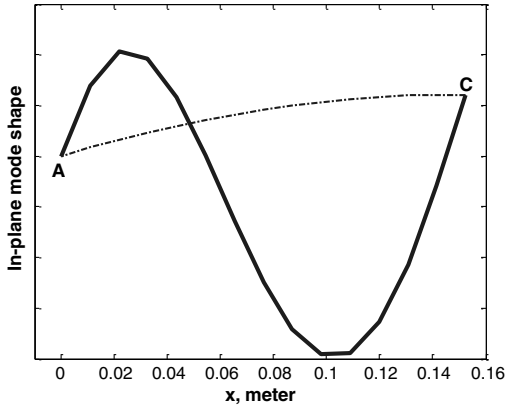

c) In-plane mode (3,1) along A-C

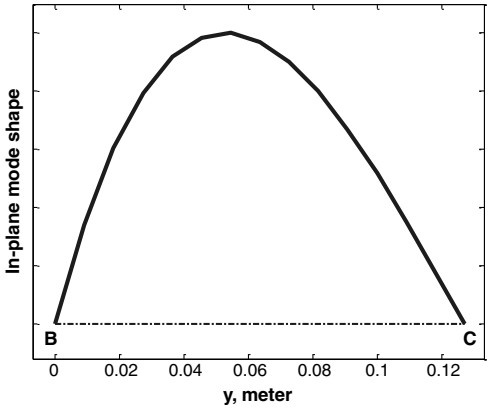

d) In-plane mode (3,1) along B-C

Fig. 4 Bending and in-plane mode shapes of mode (3,1) for a quarter of the simply supported $[0_3/90_3]$ cylindrical panel along A–C and B–C in Fig. 1.

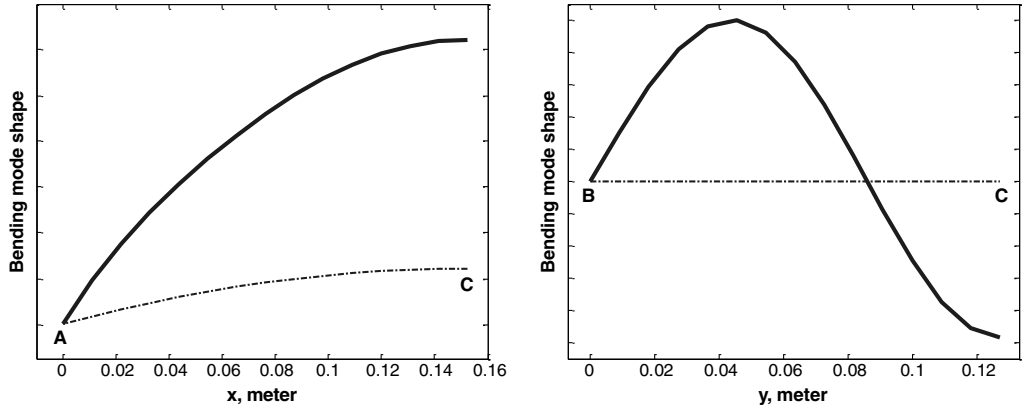

a) Bending mode (1,3) along A-C

b) Bending mode (1,3) along B-C

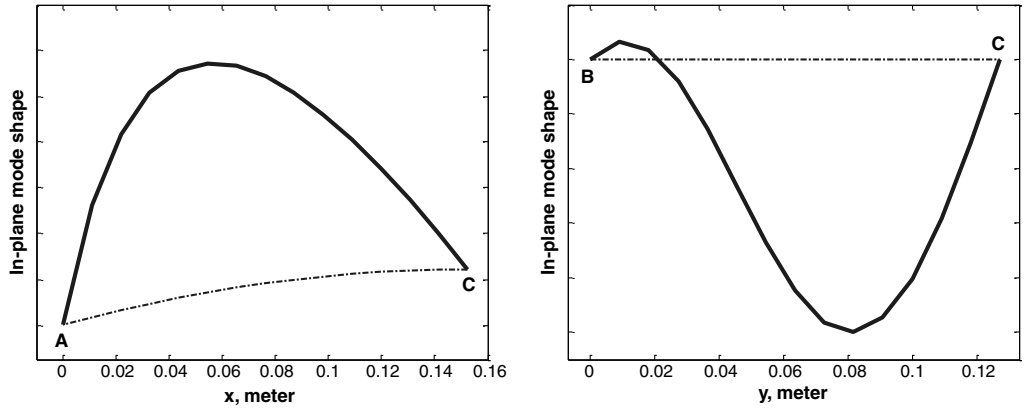

c) In-plane mode (1,3) along A-C

d) In-plane mode (1,3) along B-C

Fig. 5 Bending and in-plane mode shapes of mode (1,3) for a quarter of the simply supported $[0_3/90_3]$ cylindrical panel along A–C and B–C in Fig. 1.

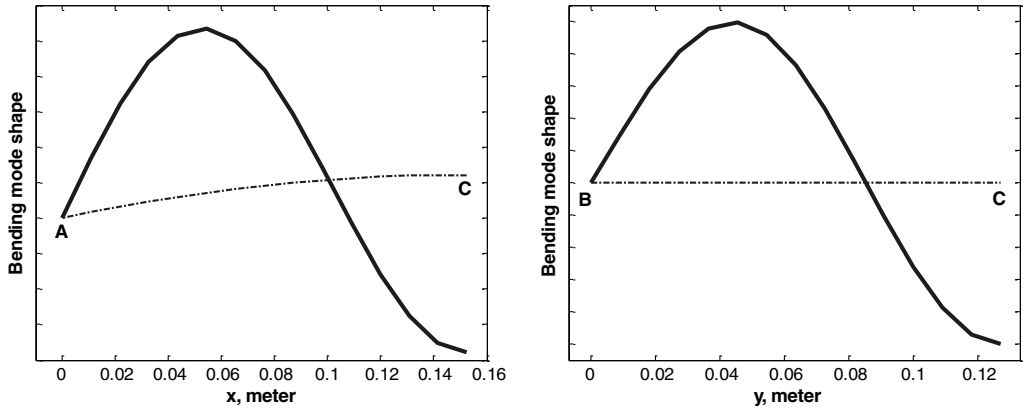

a) Bending mode (3,3) along A-C

b) Bending mode (3,3) along B-C

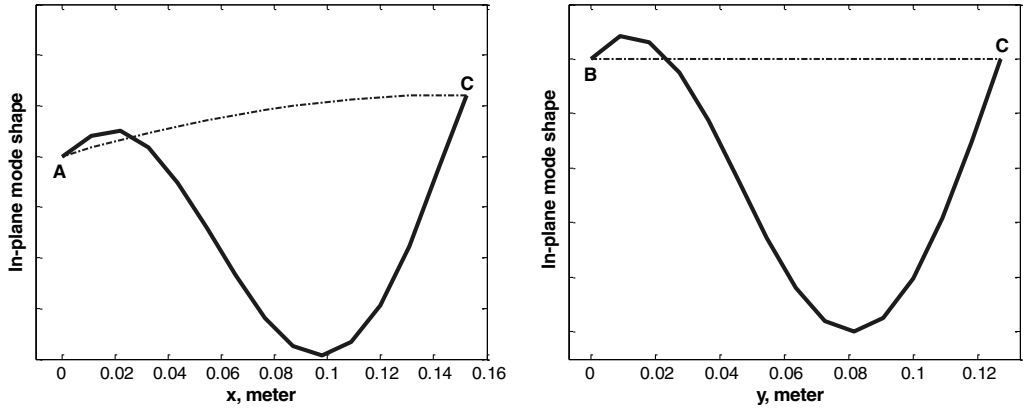

c) In-plane mode (3,3) along A-C

d) In-plane mode (3,3) along B-C

Fig. 6 Bending and in-plane mode shapes of mode (1,1) for a quarter of the simply supported $[0_3/90_3]$ cylindrical panel along A–C and B–C in Fig. 1.

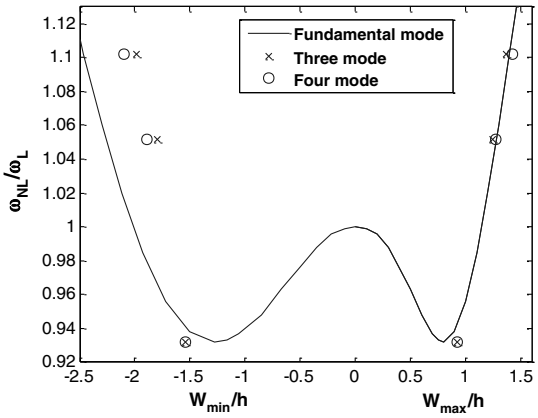

Fig. 7 Multiple-mode and single-mode solutions for the $[0_3/90_3]$ cylindrical panel.

$$\omega = \sqrt{s_1^2 + s_2^2} \tag{51}$$

In the current system, the preceding frequency corresponds to the LCO frequency of the shallow shell. As mentioned earlier, this frequency detected from the ARX model is based on the deflection $W_{\max}$ of the periodic LCO response, i.e., it is computed using the stiffness matrix having its contributions from the linear and nonlinear components, as introduced in Eq. (17). Finally, the LCO period can be calculated as

$$T_p = \frac{2\pi}{\omega} \tag{52}$$

C. Nonlinear Controller Using LQR/EKF with System ID

LQR/EKF has a good control performance for nonlinear free-vibration with a certain nonlinear frequency. However, if the system response frequency is suddenly changed, it is not possible to control the vibrations only with the LQR/EKF. Thus, the LQR/EKF enhanced with the system ID is effectively feasible to suppress not only the original LCO but also the changed LCO. The procedure using a system ID consists of two steps: First, the system ID detects the nonlinear frequency of LCO from the output through the nonlinear system. Then, the detected frequency is identified by using the relationship between the nonlinear frequency and vibration amplitude. Secondly, the system ID provides the identified frequency to LQR/EKF controller. The frequency information given by the system ID adjusts the control parameters of the LQR/EKF controller, i.e., the LQR/EKF controller with the system ID is optimized based on the corresponding updated system.

IV. Numerical Results and Discussion

The FE modal equations of motion of the laminated composite shallow shell can be solved by the shooting method and the fourth order Runge-Kutta integration scheme to obtain the LCO. For multiple-mode solutions, a selection of proper initial conditions is critical for obtaining the steady periodic response. In the present work, the iterative procedure presented by Przekop et al. [28] is used to provide such an initial conditions.

In general, it was demonstrated that nonsymmetric dynamic response can exist for symmetric structures exposed to a symmetric spatial loading distribution [29,30]. However, for the structure under consideration in response regimes $W_{\max}/h$ comparable with the current studies, it was found [9] that the antisymmetric response components are not present. Consequently, the reduced-order model used in this study is based only on the symmetric modes.

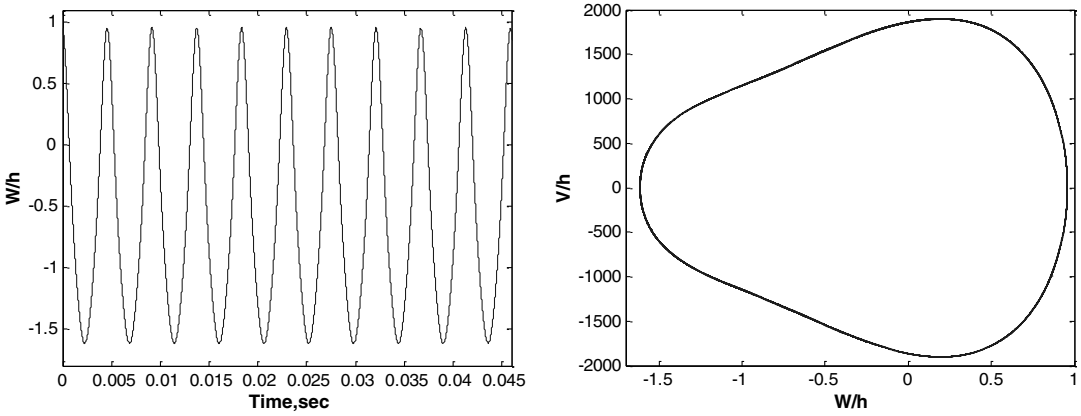

Fig. 8 Time response and phase plot of the panel with embedded MFC having the largest softening effect.

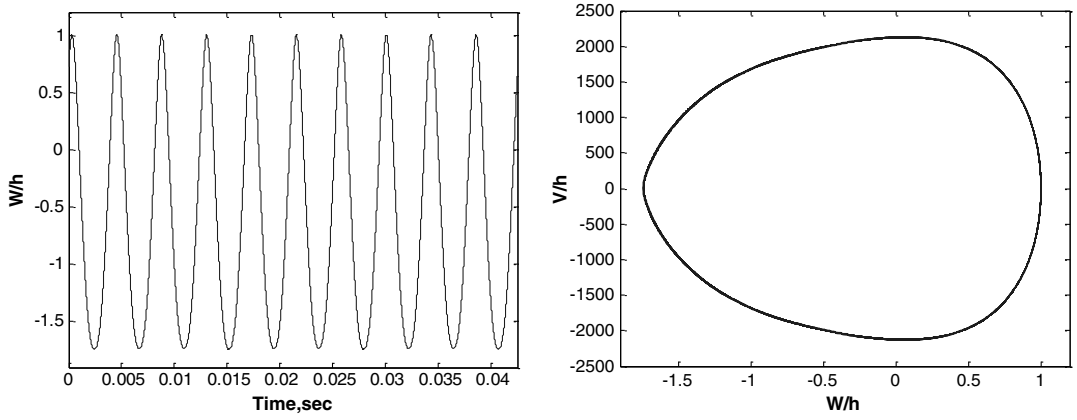

Fig. 9 Time response and phase plot of the panel with embedded PZT5A having the largest softening effect.

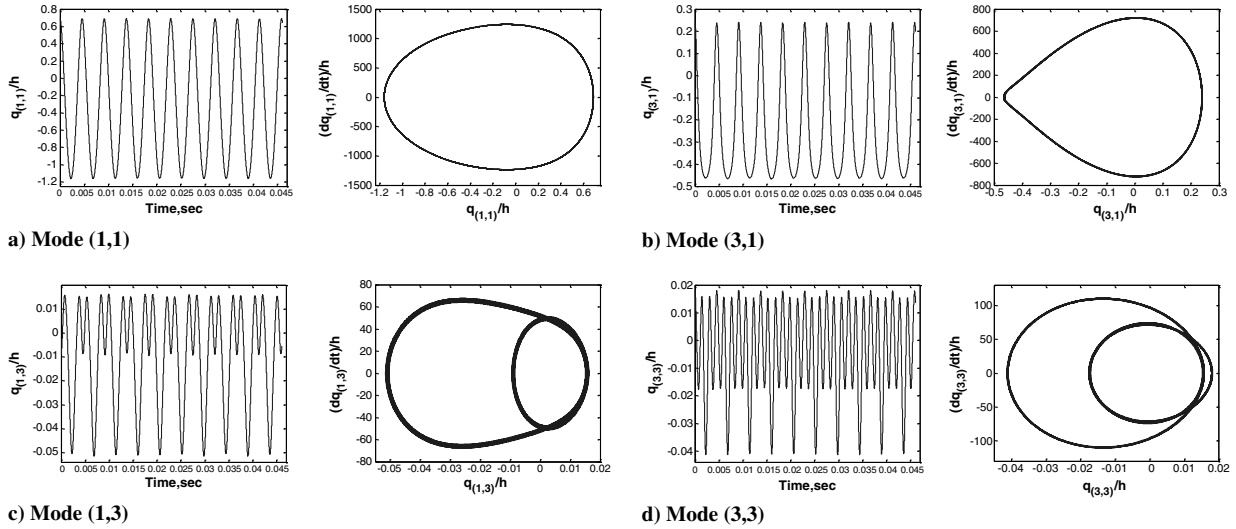

a) Mode (1,1) **b) Mode (3,1)**

c) Mode (1,3) **d) Mode (3,3)**

Fig. 10 For modes (1,1), (3,1), (1,3), and (3,3), time response and phase plots of the panel with embedded MFC having the largest softening effect.

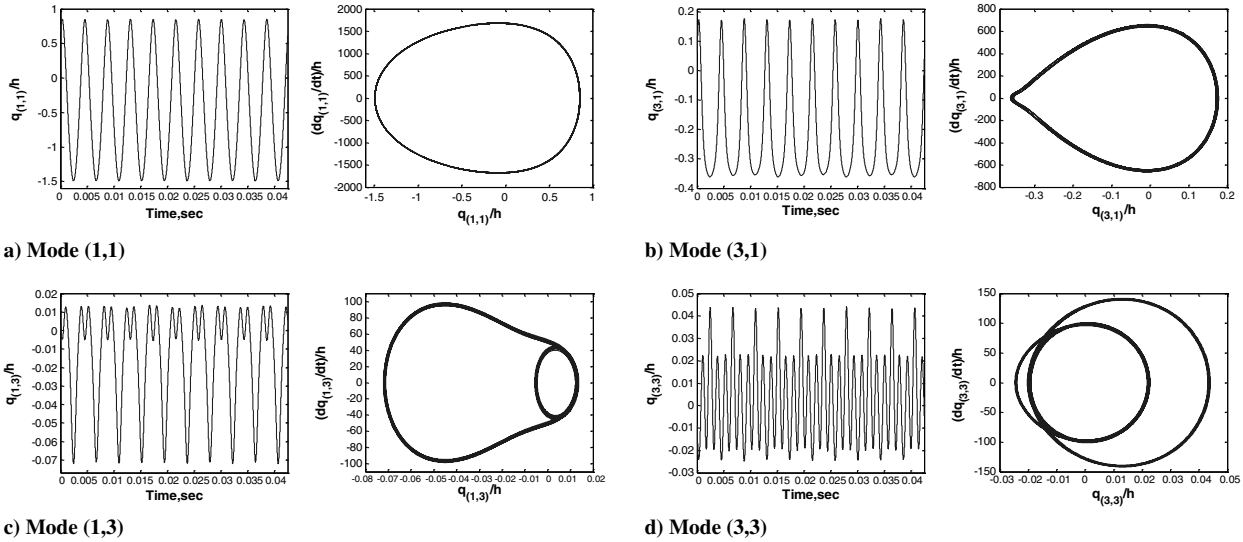

a) Mode (1,1) **b) Mode (3,1)**

c) Mode (1,3) **d) Mode (3,3)**

Fig. 11 For modes (1,1), (3,1), (1,3), and (3,3), time response and phase plots of the panel with embedded PZT5A having the largest softening effect.

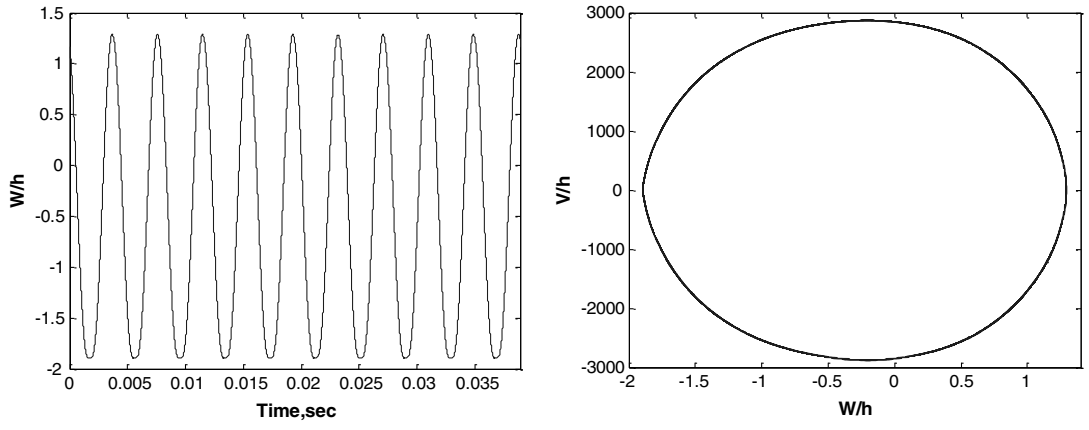

Fig. 12 Time response and phase plot for the $[0_3/90_3]$ cylindrical panel with embedded MFC having only the hardening effect.

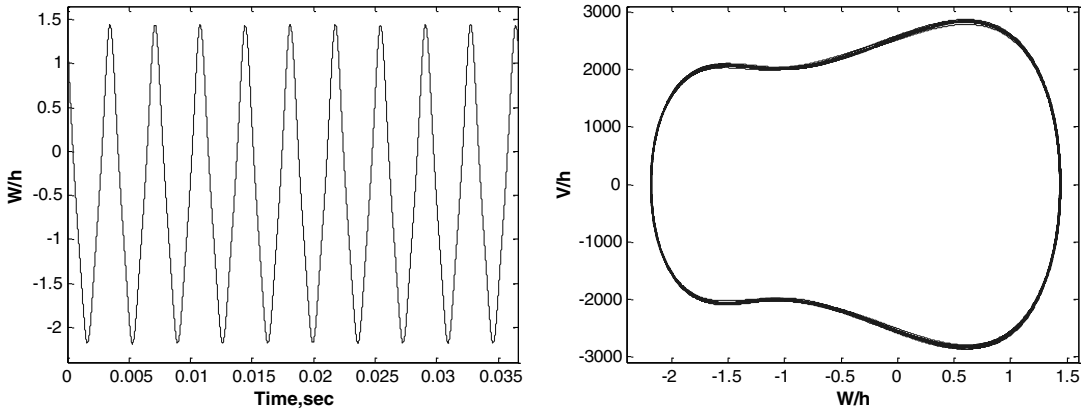

Fig. 13 Time response and phase plot for the $[0_3/90_3]$ cylindrical panel with embedded PZT5A having only the hardening effect.

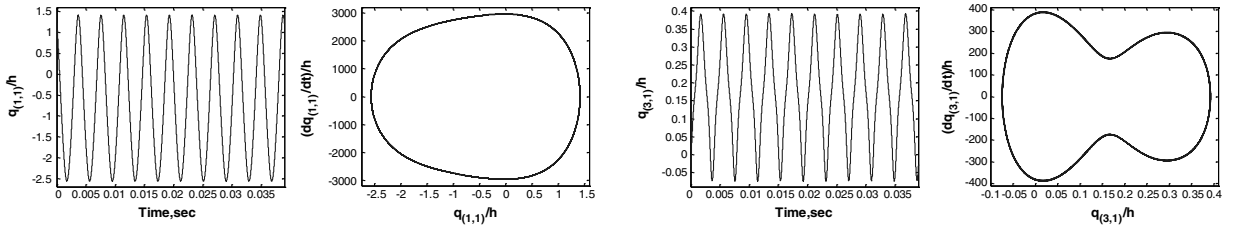

a) Mode (1,1) **b) Mode (3,1)**

c) Mode (1,3) **d) Mode (3,3)**

Fig. 14 For modes (1,1), (3,1), (1,3), and (3,3), time response and phase plots for the $[0_3/90_3]$ cylindrical panel with embedded MFC having only the hardening effect.

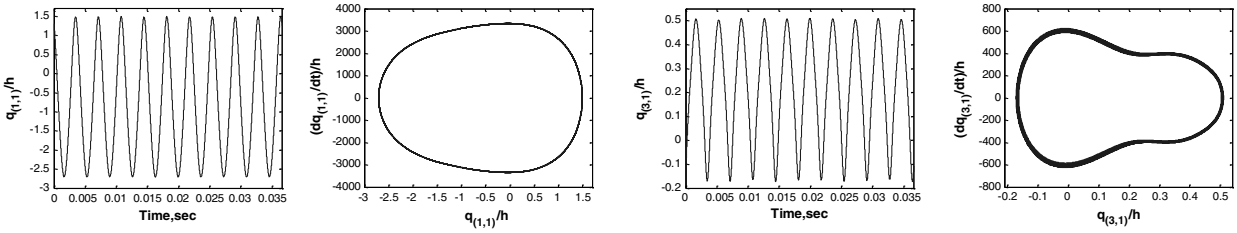

a) Mode (1,1) **b) Mode (3,1)**

c) Mode (1,3) **d) Mode (3,3)**

Fig. 15 For modes (1,1), (3,1), (1,3), and (3,3), time response and phase plots for the $[0_3/90_3]$ cylindrical panel with embedded PZT5A having only the hardening effect.

Table 2 Modal participations in the three-mode solutions for a simply supported $[0_3/90_3]$ cylindrical rectangular panel with embedded actuators

$\frac{\omega_{NL}}{\omega_L}$	$\frac{W_{max}}{h}$ $\frac{W_{min}}{h}$	Modal participation at W_{max}, % Modal participation at W_{min}, %		
		q_{11}	q_{31}	q_{13}
Graphite/epoxy with MFC				
0.9318	0.9212	73.4644	25.3141	1.2215
0.9318	−1.5389	69.2581	27.6468	3.0951
1.0516	1.2425	93.9060	5.0851	1.0089
1.0516	−1.7931	80.3475	14.1415	5.5110
1.1022	1.3705	95.0354	4.1700	0.7946
1.1022	−1.9864	81.4720	12.8384	5.6896
Graphite/epoxy with PZT5A				
0.9387	1.0356	82.7397	16.2571	1.0032
0.9387	−1.7958	77.6370	18.5975	3.7655
1.1039	1.3894	90.8526	9.0576	0.0897
1.1039	−2.0556	79.4488	15.1691	5.3821

Table 3 Modal participations in the four-mode solutions for a simply supported $[0_3/90_3]$ cylindrical rectangular panel with embedded actuators

$\frac{\omega_{NL}}{\omega_L}$	$\frac{W_{max}}{h}$ $\frac{W_{min}}{h}$	Modal participation at W_{max}, % Modal participation at W_{min}, %			
		q_{11}	q_{31}	q_{13}	q_{33}
Graphite/epoxy with MFC					
0.9318	0.9227	72.2108	24.9282	0.9762	1.8848
0.9318	−1.5404	67.6730	26.9938	2.9480	2.3852
1.0516	1.2775	90.1101	5.6963	0.9028	3.2908
1.0516	−1.8898	78.3496	13.5415	5.2680	2.8408
1.1022	1.4206	90.1556	4.6593	0.8320	4.3531
1.1022	−2.1031	79.2025	12.1189	5.3151	3.3635
Graphite/epoxy with PZT5A					
0.9387	1.0042	80.9464	16.2645	0.4845	2.3046
0.9387	−1.7409	76.1459	18.0289	3.6274	2.1978
1.0880	1.4467	84.3437	9.3753	0.8350	5.4460
1.0880	−2.1879	76.7023	14.3507	4.8012	4.1459

Furthermore, due to the symmetry of the response, only a quarter of the shell was modeled using a 14×14 mesh or 392 triangular shallow-shell elements. Simply supported immovable boundary conditions were applied on the two constrained edges and symmetry conditions were prescribed on the remaining two edges. For all study cases, graphite-epoxy cylindrical panels presented in Fig. 1 are used. The panel's dimensions are $12 \times 10 \times 0.054$ in.. ($30.48 \times 25.40 \times 0.1372$ cm) with the curvatures of $R_x = 150$ in. (381 cm) and $R_y = \infty$, and the symmetry axes connecting points A, C and B indicate the preceding quarter-panel section studied. Two antisymmetrical lamination stacking sequences of [0/0/0/90/90/90] and [90/90/90/0/0/0] (shorthand notation $[0_3/90_3]$ and $[90_3/0_3]$, respectively) were considered. Therefore per Eq. (5), the laminate stiffness $[B]$ adopts nonzero values indicative of bending-in-plane material coupling.

The MFC and the traditional piezoelectric materials (PZT5A) are used as self-sensing actuators. All material properties are shown in Table A1. Before the suppression of nonlinear vibrations is

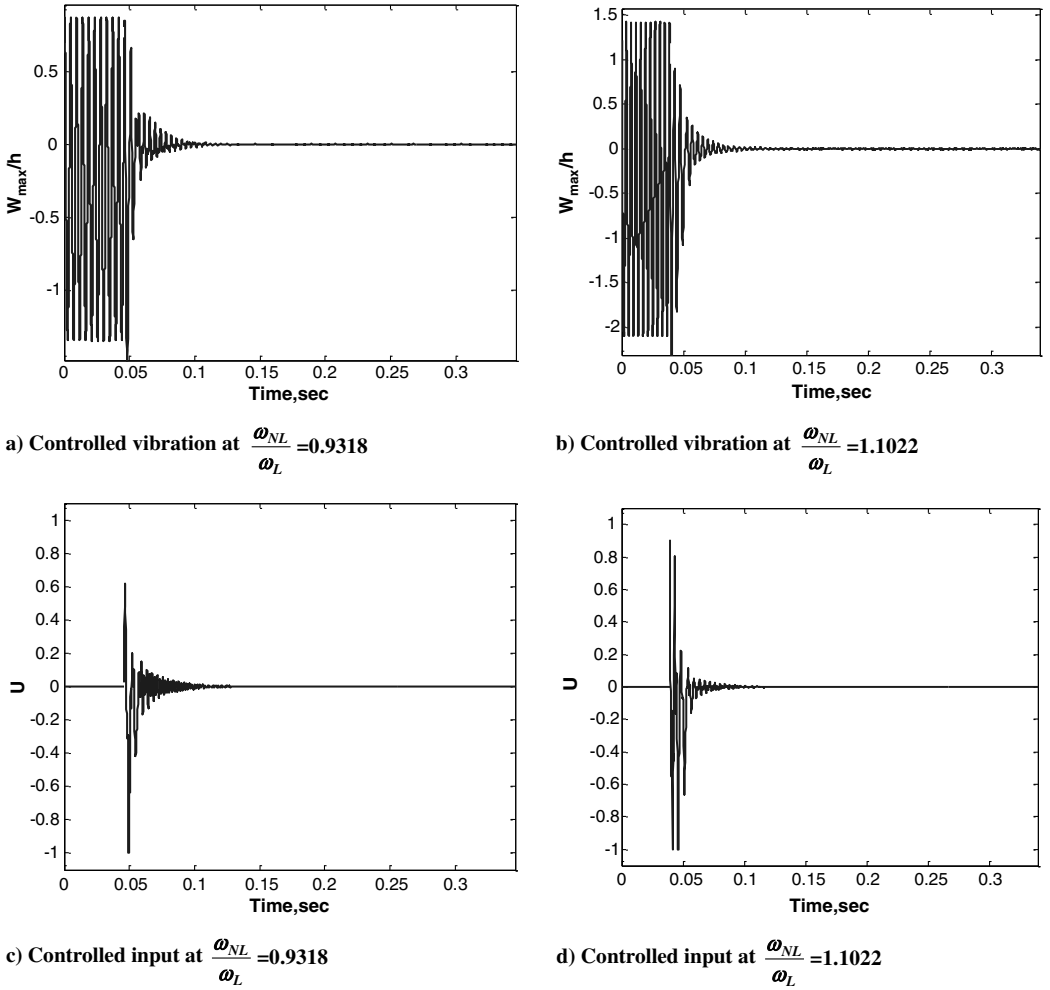

a) Controlled vibration at $\frac{\omega_{NL}}{\omega_L}$ =0.9318

b) Controlled vibration at $\frac{\omega_{NL}}{\omega_L}$ =1.1022

c) Controlled input at $\frac{\omega_{NL}}{\omega_L}$ =0.9318

d) Controlled input at $\frac{\omega_{NL}}{\omega_L}$ =1.1022

Fig. 16 Performance of the active controller for the 4-mode solution of the simply supported $[0_3/90_3]$ cylindrical panel using MFC.

attempted, the relation of the large-amplitude LCO deflection versus the nonlinear frequency was investigated. Then, the control results for an active and adaptive controller are introduced and discussed.

A. Finite-Element Free-Vibration Analysis Results

This section includes not only results of the plain graphite-epoxy panel studies but also free-vibration results for panels with embedded PZT5A and MFC piezoelectric materials.

1. Lamination Stacking Sequence Influence on the Response Characteristics

Since the softening effect in curved panels can be either magnified or suppressed by the lamination stacking sequence selection, the response of curved panels with two different antisymmetric lamination stacking sequences of $[0_3/90_3]$ and $[90_3/0_3]$ is investigated first with a single-mode solution. Although the single-mode solution may be not very accurate, it is usually sufficient to determine the presence of the softening and/or hardening response characteristic [9]. It was determined from the single-mode analysis that the lamination stacking sequence of $[0_3/90_3]$ (where the $[0_3]$ layers are closer to the shell center) exhibits both softening and hardening response characteristics. Contrary, the $[90_3/0_3]$ shallow-shell panel exhibits only the hardening response as shown in Fig. 2. Consequently, the $[0_3/90_3]$ lamination was selected for the further studies since the presence of two distinct types of nonlinearity constituted a more challenging case for the control system design.

2. Natural Frequencies and Mode Shapes

To obtain an accurate large-amplitude free-vibration response, a multimode analysis rather than a single-mode analysis may be necessary. Generally, the larger the amplitude, the larger the number of modes required for the converged solution. In this study, the number of modes is increased up to four, and includes the lowest frequency symmetric modes (1,1), (3,1), (1,3), and (3,3). The first four natural frequencies of the composite cylindrical panel with and without the actuators are presented in Table 1. For a curved panel, since the transverse displacement component and the in-plane displacement component of each linear mode are inherently coupled, both transverse and in-plane mode-shape components for the $[0_3/90_3]$ lamination panel are shown in Figs. 3–6 along A–C and B–C shell sections, as depicted in Fig. 1.

3. Multimode Free-Vibration Solutions

Figure 7 shows that the difference between the three-mode and the four-mode solutions in softening part is relatively insignificant, which is usually indicative of adequate convergence being achieved. Also, it is demonstrated that the multimode solutions depart from the single-mode solution, especially for larger amplitudes in the inbound part of the oscillation. Time responses and phase plots for the simply supported $[0_3/90_3]$ cylindrical rectangular panel under moderately large-amplitude free vibrations, which have the largest softening effect or the lowest frequency ratio $\omega_{\mathrm{NL}}/\omega_L$, are shown in Fig. 8 for the panel embedded with MFC and in Fig. 9 for the panel embedded with PZT5A. The time response and phase plot of each mode are presented in Fig. 10 for the MFC-embedded panels, and Fig. 11 for PZT5A embedded panels.

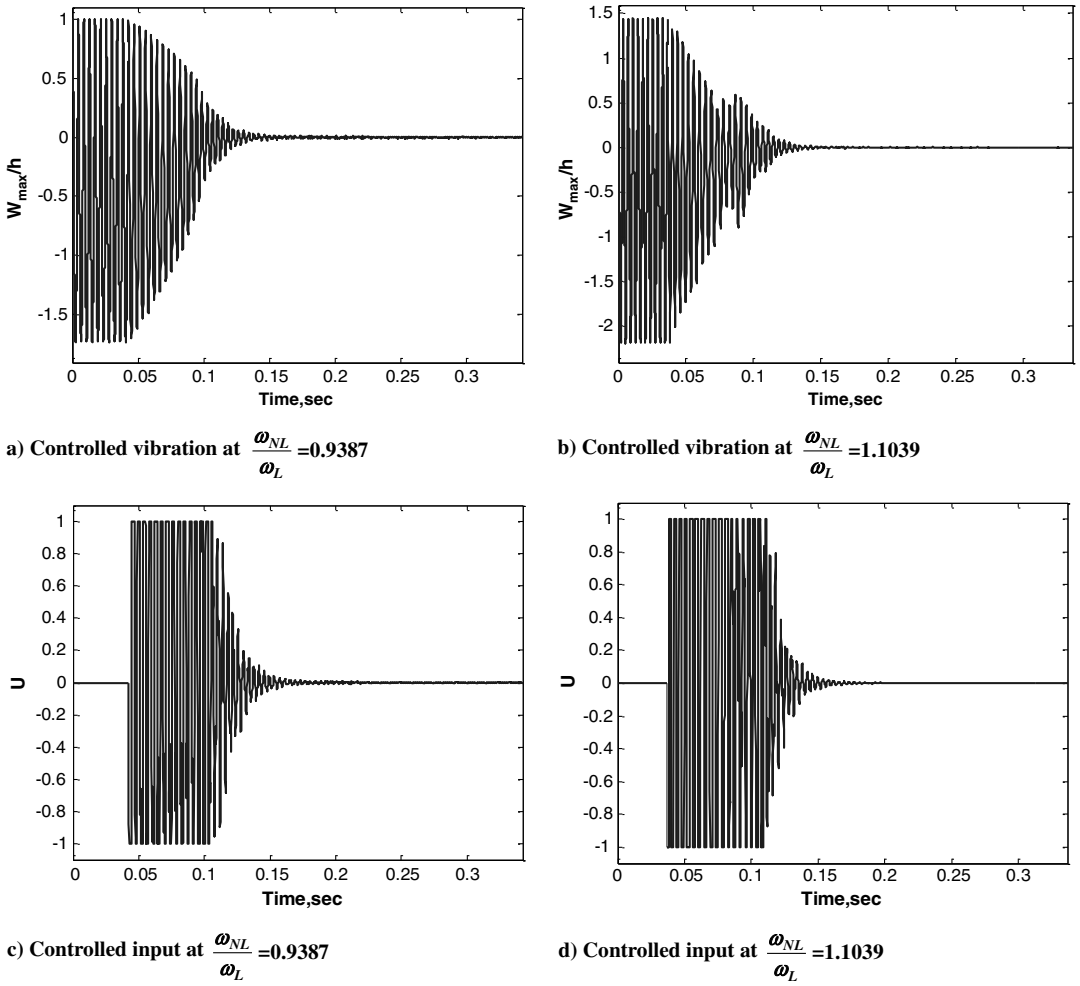

a) Controlled vibration at $\frac{\omega_{NL}}{\omega_L}$ =0.9387

b) Controlled vibration at $\frac{\omega_{NL}}{\omega_L}$ =1.1039

c) Controlled input at $\frac{\omega_{NL}}{\omega_L}$ =0.9387

d) Controlled input at $\frac{\omega_{NL}}{\omega_L}$ =1.1039

Fig. 17 Performance of the active controller for the 4-mode solution of the simply supported $[0_3/90_3]$ cylindrical panel using PZT5A.

The results for the $[0_3/90_3]$ composite cylindrical panel in the response range having only the hardening effect are presented in Fig. 12 for the panel embedded with MFC, and in Fig. 13 for the panel embedded with PZT5A. The corresponding time response and phase plot for each mode are illustrated in Fig. 14 for MFC and Fig. 15 for PZT5A.

The modal participation of each mode can be calculated based on Eq. (19). The inbound deflection of the shallow shell has a larger absolute value than the outbound deflection, while the absolute values of the inbound deflection of the flat plate are the same as the outbound deflection. For this reason, modal participations for both $W_{\max}/h$ and $W_{\min}/h$ displacement ratios are computed. Tables 2 and 3 show that the modal participations at $W_{\max}/h$ and $W_{\min}/h$ are different for both the three-mode and the four-mode solution, respectively.

B. Control Results for Nonlinear Free Vibrations

1. *Optimal Placement of Self-Sensing Piezoelectric Actuators*

Before applying an active or an adaptive controller, the best location of the embedded piezoelectric layers should be first investigated to attain the optimal actuation, optimal sensing, and especially important in aerospace applications, minimal weight. The NFCG method in Eq. (25) and the NKFEG method in Eq. (32) are used to find the optimized locations for actuators and sensors, respectively. The preferable locations of actuators and sensors obtained from the NFCG and NKFEG method are then combined for the best location of self-sensing actuators.

The optimal placement of actuators and sensors using not only MFC but also PZT5A is shown in Figs. B1–B4 in Appendix B. The optimal location of self-sensing actuators for both actuator materials is illustrated in Figs. B5 and B6 in Appendix B. In this study, the optimal size of self-sensing actuators is investigated with 20.41% of the panel area. The optimal location of MFC is determined where NFCG norm $\|K\| > 4.265$ and NKFEG norm $\|K_e\| > 2.198$, and the optimal location of PZT5A is obtained using NFCG norm $\|K\| > 4.195$ and NKFEG norm $\|K_e\| > 0.015$.

2. *Active Control Results*

Before investigating the performance of the adaptive controller, the performance of the active LQR/EKF controller is first determined and discussed in this section. Although the active controller has a good control performance at a certain nonlinear frequency, when the frequency of LCO is suddenly changed, such a controller is no longer suitable. To deal with this sudden change of the system response, LQR/EKF controller should be adaptively designed. The adaptive control performance will be discussed in the next section.

For an active LQR/EKF controller using MFC, designed parameters of $\boldsymbol{Q}$ and $\boldsymbol{R}$ weighting matrices for LQR with $\boldsymbol{Q_e}$ and $\boldsymbol{R_e}$ weighting matrices for EKF are chosen as

$$\boldsymbol{Q} = c \times \begin{bmatrix} \omega_r & 0 \\ 0 & \omega_r \end{bmatrix}, \qquad \boldsymbol{R} = [\boldsymbol{C}][\boldsymbol{C}]^T \tag{53}$$

$$\boldsymbol{Q_e} = c \times [\boldsymbol{I}], \qquad \boldsymbol{R_e} = [\boldsymbol{C}][\boldsymbol{C}]^T \tag{54}$$

Designed parameters of an active controller using PZT5A are selected as

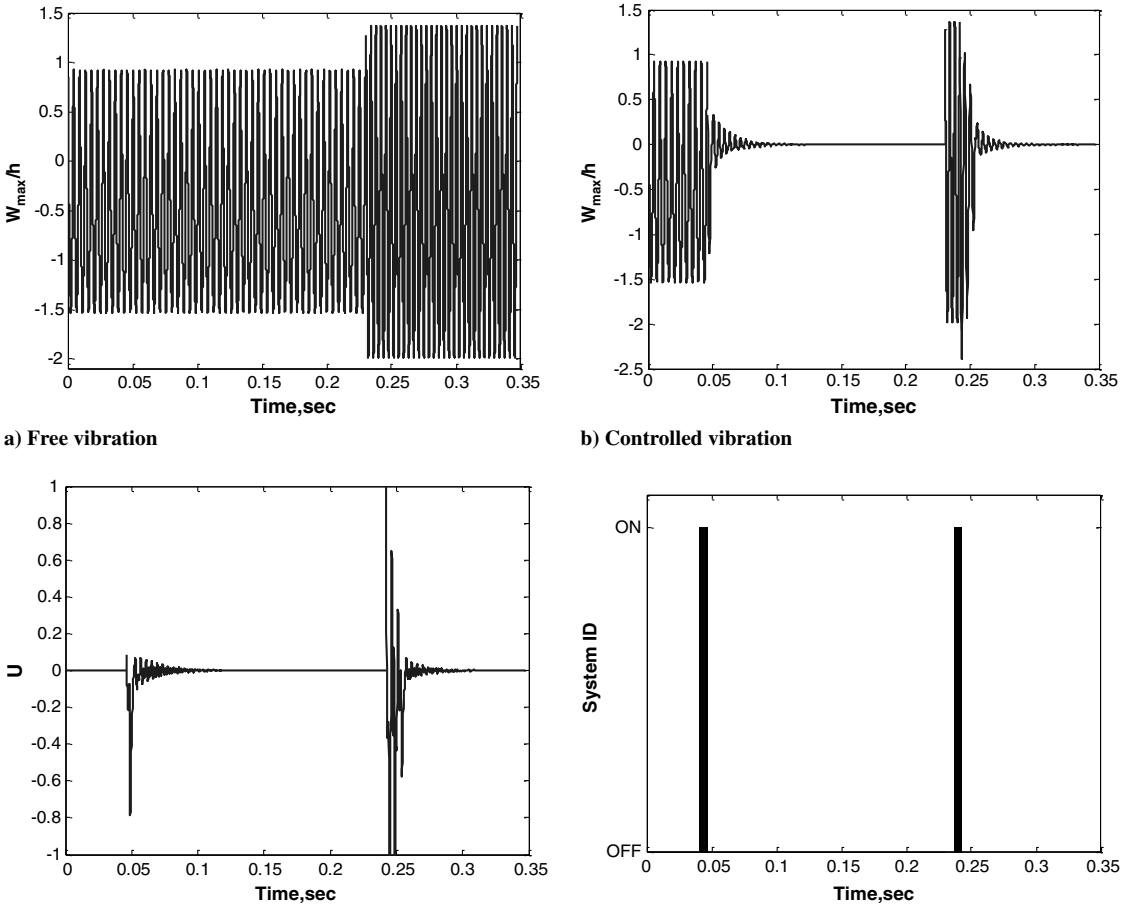

Fig. 18 Performance of the adaptive controller for the 4-mode solution of the simply supported $[0_3/90_3]$ cylindrical panel using MFC at $\frac{\omega_{\mathrm{NL}}}{\omega_L} = 0.9318$ and $\frac{\omega_{\mathrm{NL}}}{\omega_L} = 1.1022$.

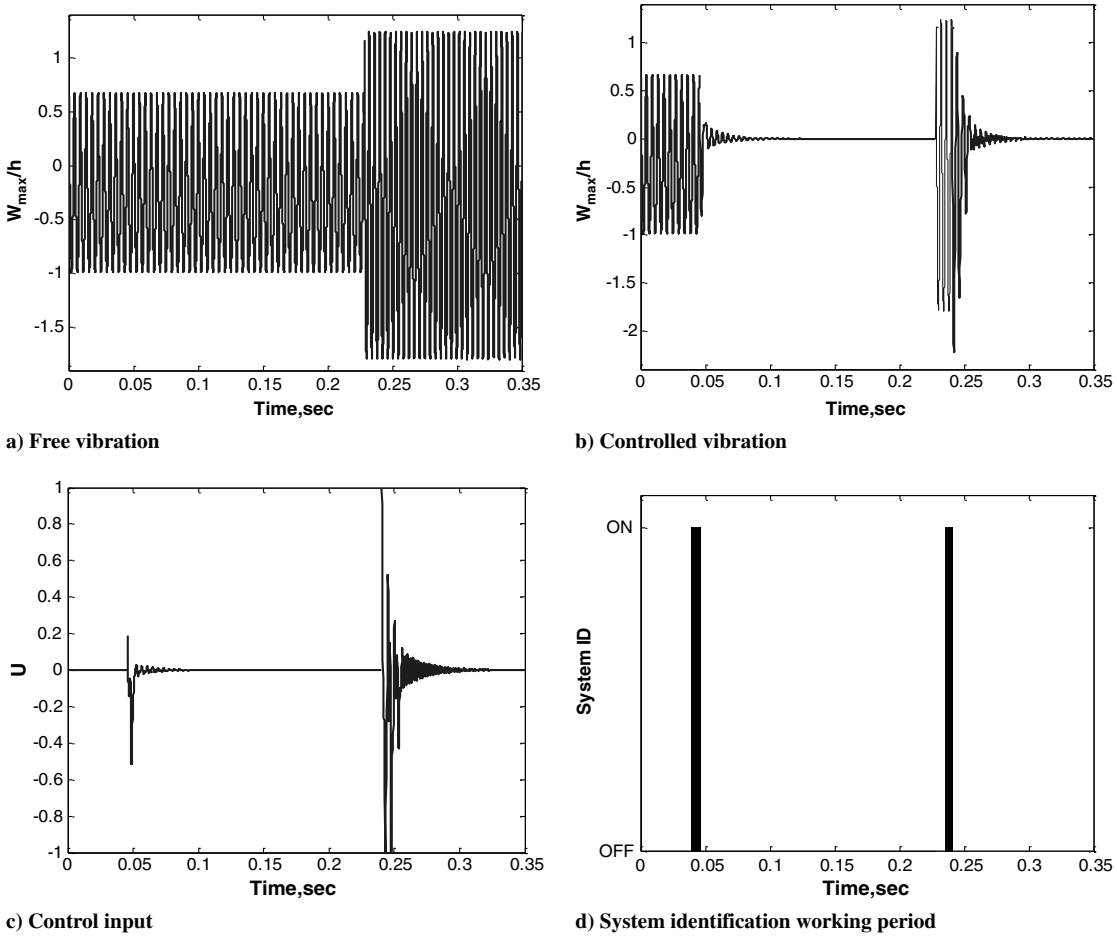

Fig. 19 Performance of adaptive controller for the 4-mode solution of the simply supported $[0_3/90_3]$ cylindrical panel using MFC at $\frac{\omega_{NL}}{\omega_L} = 0.9418$ and $\frac{\omega_{NL}}{\omega_L} = 1.0516$.

$$\boldsymbol{Q} = c \times \begin{bmatrix} \omega_r & 0 \\ 0 & \omega_r \end{bmatrix}, \qquad \boldsymbol{R} = [\boldsymbol{I}] \tag{55}$$

$$\boldsymbol{Q}_e = c \times [\boldsymbol{I}], \qquad \boldsymbol{R}_e = c \times [\boldsymbol{I}] \tag{56}$$

where ω_r $(r = 1, 2, 3 \cdots n)$ are linear natural frequencies, and c is a constant number.

Figure 16 for the MFC-embedded panel, and Fig. 17 for the PZT5A-embedded panel show that active LQR/EKF controller is effective in suppressing the nonlinear vibration at a certain fixed frequency. These results indicate that the active controller using MFC has much better control performance than using PZT5A. This is why the adaptive controller, which will be discussed in the next section, is designed using only the MFC self-sensing actuator.

3. Adaptive Control Results

The active controller has difficulties to adjust the control parameters to cope with the changed structural response. The controller should thus be adaptively designed using the system ID which has the ability to identify the LCO frequency. Especially, the adaptive controller is highly suitable for the suppression of the nonlinear free vibrations of the cylindrical panel including hardening and softening characteristics.

The system identification algorithm is implemented before the controller is activated. Figure 18 shows an excellent control performance of adaptive controller which consists of a) the free vibrations with the nonlinear frequencies including the largest softening effect in this system, b) controlled vibration, c) control input, and d) the time period when the system ID is activated. Figure 19 shows that the adaptive controller has the capability to suppress a broad range of nonlinear free-vibration regimes.

V. Conclusions

A coupled structural-electrical nonlinear modal FE model for laminated composite shallow shells with embedded piezoelectric sensors and actuators was formulated in structural DOF and then transformed into the reduced-coordinates. The free response characteristics of the shallow shells were first investigated. It was determined that the curved panel with the antisymmetric lamination sequence of $[0_3/90_3]$ exhibits both softening and hardening nonlinear response characteristics, while the curved panel with the lamination sequence of $[90_3/0_3]$ provides only the hardening response behavior.

For accurate LCO analysis, a multiple-mode approach with an iterative procedure to determine the initial conditions providing a periodic response was used. The results confirmed that multiple-mode solutions instead of single-mode solutions were necessary for obtaining accurate large-amplitude LCO.

Based on the active control studies, it was determined that the LQR/EKF controller has a good control performance at a certain nonlinear frequency. Additionally, it was demonstrated that the MFC is a much more efficient actuator than the PZT5A. The active controller adequate performance, however, was found being limited to a specific fixed nonlinear frequency. Consequently, it was concluded that the LQR/EKF should be adaptively designed by using system ID algorithm to improve its robustness. Once the controller adaptability was introduced, it was demonstrated that the nonlinear vibrations of the system changing its response characteristics from the softening to hardening can be also successfully suppressed.

Appendix A: Material Properties

Table A1 Material properties of the graphite-epoxy composite, PZT5A, and MFC

Materials	Young's modulus, psi	Shear modulus, psi	Poisson's ratio	Density, lb-sec^2/in.^{4}	Charge constant, in./V	$V_{\max}$, V	Thickness, in.
Graphite-epoxy	$E_1 = 26.24 \times 10^6$	$G_{12} = 1.04 \times 10^6$	$\nu_1 = 0.28$	$\rho = 1.458 \times 10^{-4}$	——	——	——
	$E_2 = 1.49 \times 10^6$		$\nu_2 = 0.011$				
PZT5A	$E_p = 9.00 \times 10^6$	$G_p = 3.43 \times 10^6$	$\nu = 0.30$	$\rho_p = 7.10 \times 10^{-4}$	$d_{31} = -7.51 \times 10^{-9}$	820	$h_p = 0.009$
MFC	$E_{p1} = 5.29 \times 10^6$	$G_{p12} = 2.12 \times 10^6$	$\nu_{p1} = 0.25$	$\rho_p = 7.07 \times 10^{-4}$	$d_{11} = 2.09 \times 10^{-8}$	2000	$h_p = 0.009$
	$E_{p2} = 1.10 \times 10^6$	$G_{p23} = 1.06 \times 10^6$	$\nu_{p2} = 0.05$		$d_{12} = -8.27 \times 10^{-9}$		

Appendix B: Placement of Self-Sensing Actuators

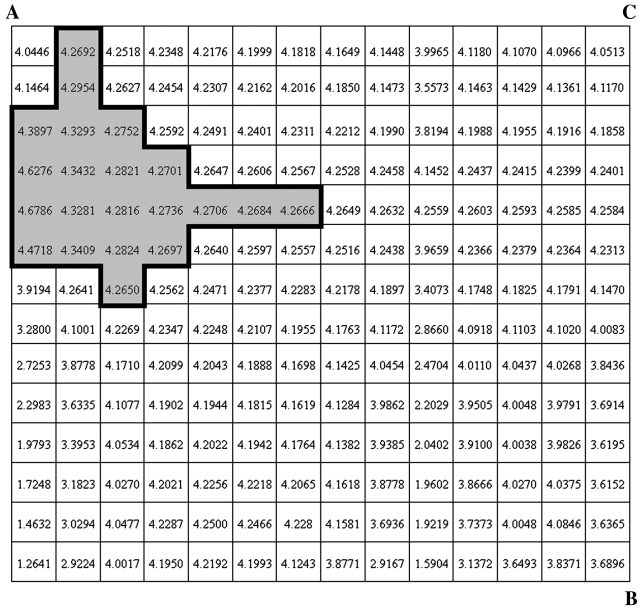

Fig. B1 NFCG norm of each element for a quarter of the composite cylindrical panel using MFC.

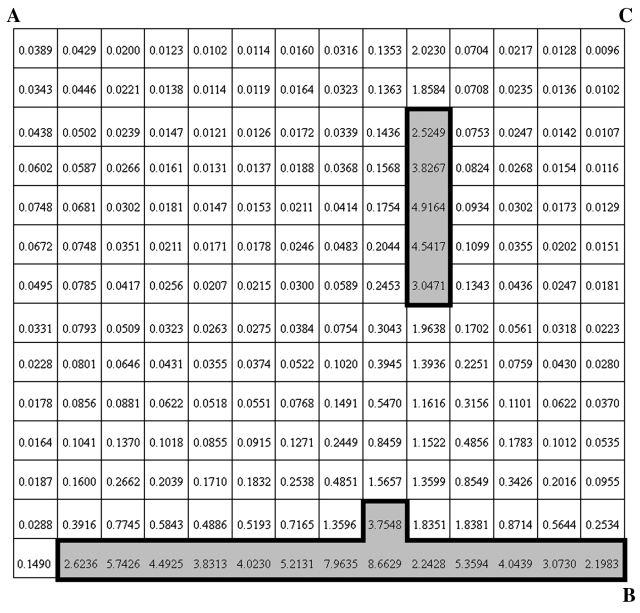

Fig. B2 NKFEG norm of each element for a quarter of the composite cylindrical panel using MFC.

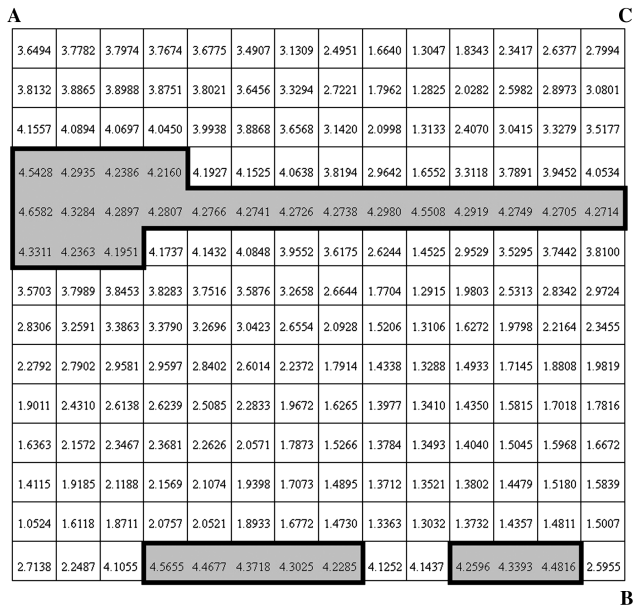

Fig. B3 NFCG norm of each element for a quarter of the composite cylindrical panel using PZT5A.

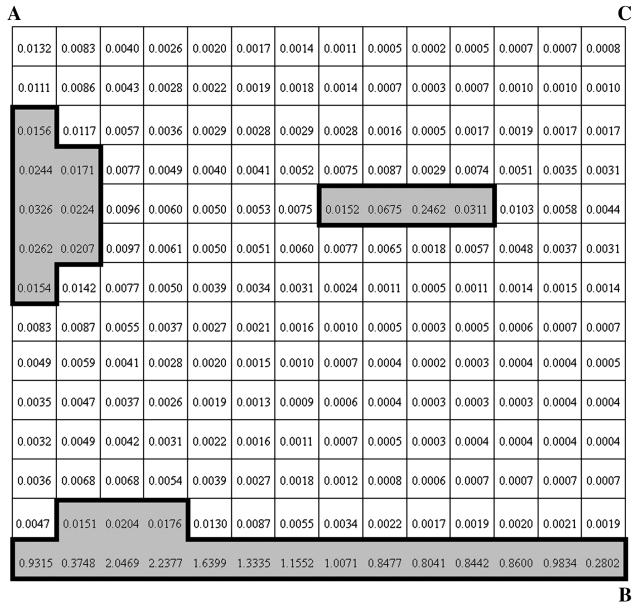

Fig. B4 NKFEG norm of each element for a quarter of the composite cylindrical panel using PZT5A.

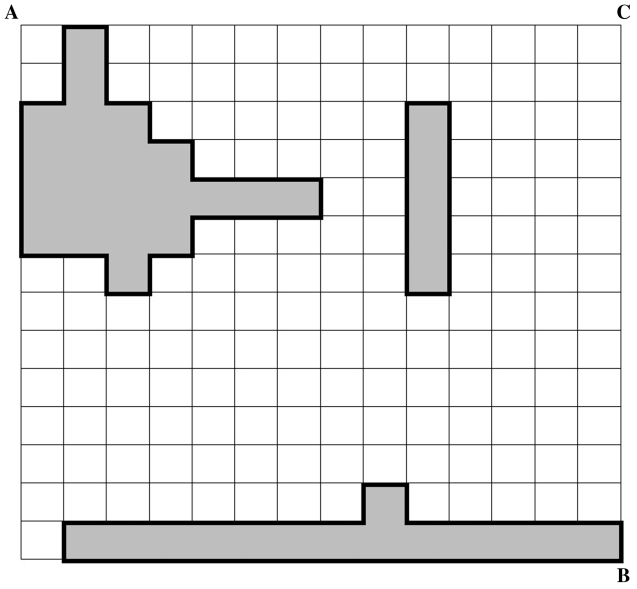

Fig. B5 The optimal locations of actuators and sensors based on NFCG and NKFEG for MFC.

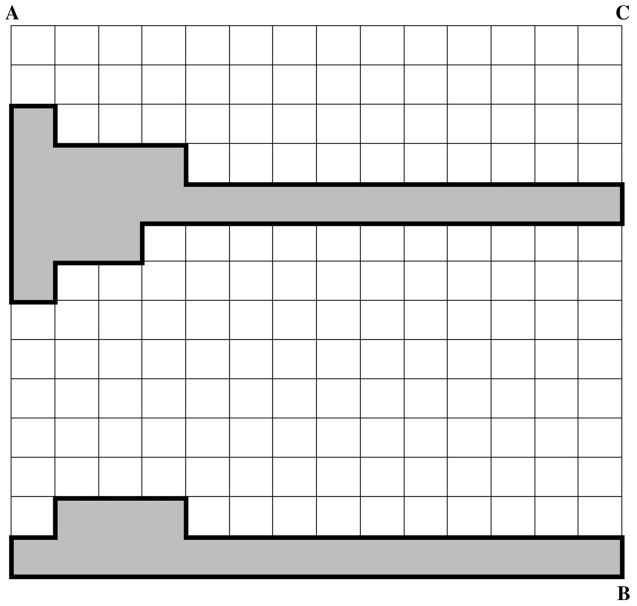

Fig. B6 The optimal locations of actuators and sensors based on NFCG and NKFEG for PZT5A.

References

[1] Liew, K. M., Lim, C. W., and Kitipornchai, S., "Vibration of Shallow Shells: A Review with Bibliography," *Applied Mechanics Reviews*, Vol. 50, No. 8, 1997, pp. 431–444. doi:10.1115/1.3101731

[2] Cummings, E. A., "Large Amplitude Vibration and Response of Curved Panels," *AIAA Journal*, Vol. 2, April 1964, pp. 709–716. doi:10.2514/3.2392

[3] Hui, D., "Influence of Geometric Imperfections and In-Plane Constraints on Nonlinear Vibrations of Simply Supported Cylindrical Panels," *Journal of Applied Mechanics*, Vol. 51, June 1984, pp. 383–390. doi:10.1115/1.3167629

[4] Raouf, R. A., and Palazotto, A. N., "On the Nonlinear Free Vibration of Curved Orthotropic Panels," *International Journal of Nonlinear Mechanics*, Vol. 29, No. 4, 1994, pp. 507–514. doi:10.1016/0020-7462(94)90019-1

[5] Abe, A., Kobayashi, Y., and Yamada, G., "Nonlinear Vibration Characteristics of Clamped Laminated Shallow Shells," *Journal of Sound and Vibration*, Vol. 234, No. 3, 2000, pp. 405–426. doi:10.1006/jsvi.1999.2877

[6] Pillai, S. R. R., and Rao, B. N., "Reinvestigation of Nonlinear Vibrations of Simply Supported Rectangular Cross-Ply Plates," *Journal of Sound and Vibration*, Vol. 160, No. 1, 1993, pp. 1–6. doi:10.1006/jsvi.1993.1001

[7] Bhimaraddi, A., "Large Amplitude Vibrations of Imperfect Antisymmetric Angle-Ply Laminated Plates," *Journal of Sound and Vibration*, Vol. 162, No. 3, 1993, pp. 457–470. doi:10.1006/jsvi.1993.1133

[8] Shi, Y., Lee, R. Y. Y., and Mei, C., "Finite Element Method for Nonlinear Free Vibration of Composite Plates," *AIAA Journal*, Vol. 35, No. 1, 1997, pp. 159–166. doi:10.2514/2.78

[9] Przekop, A., Azzouz, M. S., Guo, X., Mei, C., Shi, Y., Lee, R. Y. Y., and Mei, C., "Finite Element Multiple-Mode Approach to Nonlinear Free Vibrations of Shallow Shells," *AIAA Journal*, Vol. 42, No. 11, 2004, pp. 2373–2381. doi:10.2514/1.483

[10] Inman, D. J., "Active Modal Control for Smart Structures," *Philosophical Transactions: Mathematics, Physical and Engineering Sciences*, Vol. 359, No. 1778, Jan. 2001, pp. 205–219. doi:10.1098/rsta.2000.0721

[11] Zhang, J. F., "Optimal Control for Mechanical Vibration Systems Based on Second-Order Matrix Equations," *Mechanical Systems and Signal Processing*, Vol. 16, No. 1, 2002, pp. 61–67. doi:10.1006/mssp.2001.1441

[12] Xie, S. L., Zhang, X. N., Zhang, J. H., and Yu, L., "H_∞ Robust Vibration Control of a Thin Plate Covered with a Controllable Constrained Damping Layer," *Journal of Vibration and Control*, Vol. 10, No. 1, 2004, pp. 115–133. doi:10.1177/1077546304032994

[13] Abdel-Motagaly, K., and Mei, C., "On the Control of Nonlinear Free Vibrations of a Simply Supported Beam," *The 39th AIAA/ASME/ASCE/AHS/ASC Structures, Structural Dynamics and Materials Conference*, Long Beach, CA, April 1998, pp. 3266–3278.

[14] De Abreu, G. L. C. M., and Ribeiro, J. F., "A Self-Organizing Fuzzy Logic Controller for the Active Control of Flexible Structures Using Piezoelectric Actuators," *Applied Soft Computing*, Vol. 1, No. 4, 2002, pp. 271–283. doi:10.1016/S1568-4946(02)00020-0

[15] Hossian, M. A., Madkour, A. A. M., Dahal, K. P., and Yu, H., "Intelligent Active Vibration Control for a Flexible Beam System," *Proceeding of the IEEE SMC UK-RI Chapter Conference 2004 on Intelligent Cybernetic Systems*, Londonderry, England, U.K., Sept. 2004, pp. 85–89.

[16] Li, Q., Phairoh, T., Huang, J. K., and Mei, C., "Adaptive Control of Nonlinear Free Vibrations of Composite Plates Using Piezoelectric Actuators," *AIAA Journal*, Vol. 44, No. 6, 2006, pp. 1169–1180. doi:10.2514/1.19673

[17] Anderson, E. H., and Hagood, N. W., "Simultaneous Piezoelectric Sensing/Actuation: Analysis and Application to Controlled Structures," *Journal of Sound and Vibration*, Vol. 174, No. 5, 1994, pp. 617–639. doi:10.1006/jsvi.1994.1298

[18] Azzouz, M. S., Mei, C., Bevan, J. S., and Ro, J. J., "Finite Element Modeling of MFC/AFC Actuators and Performance of MFC," *Journal of Intelligent Material Systems and Structures*, Vol. 12, No. 9, 2001, pp. 601–612. doi:10.1177/10453890122145384

[19] Kim, M., Li, Q., Huang, J.-K., and Mei, C., "Dynamic Active Control of Nonlinear Panel Flutter Using Aeroelastic Modes and Piezoelectric Actuators," *AIAA Journal*, Vol. 46, No. 3, March 2008, pp. 733–743. doi:10.2514/1.33803

[20] Zhou, R. C., "Finite Element Analysis for Nonlinear Flutter Suppression of Composite Panels at Elevated Temperatures Using Piezoelectric Material," Ph.D. Dissertation, Old Dominion Univ., Norfolk, VA, 1994.

[21] Tessler, A., "A C0–Anisoparametric Three-Node Shallow Shell Element," *Computer Methods in Applied Mechanics and Engineering*, Vol. 78, No. 1, 1990, pp. 89–103. doi:10.1016/0045-7825(85)90114-8

[22] Tessler, A., and Hughes, T., "A Three-Node Mindlin Plate Element with Improved Transverse Shear," *Computer Methods in Applied Mechanics and Engineering*, Vol. 50, No. 1, 1985, pp. 71–101. doi:10.1016/0045-7825(85)90114-8

[23] Abdel-Motagaly, K., Guo, X., Duan, B., and Mei, C., "Active Control of Nonlinear Panel Flutter Under Yawed Supersonic Flow," *AIAA Journal*, Vol. 43, No. 3, 2005, pp. 671–680. doi:10.2514/1.13840

[24] Park, M., "Adaptive Control of Large Amplitude Nonlinear Free Vibrations of Composite Shallow Shells Using System Identification and Self-Sensing Piezoelectric Actuators," M.S. Thesis, Dept. of Aerospace Engineering, Old Dominion Univ., Norfolk, VA, May 2008.

[25] Chen, C.-W., Huang, J.-K., Phan, M., and Juang, J.-N., "Integrated System Identification and State Estimation of Large Flexible Structures," *Journal of Guidance, Control, and Dynamics*, Vol. 15, No. 1, Jan. 1992, pp. 88–95. doi:10.2514/3.20805

[26] Phan, M., Horta, L. G., Juang, J.-N., and Longman, R. W., "Linear System Identification via an Asymptotically Stable Observer," NASA TP 3164, 1992.

[27] Juang, J. N., *Applied System Identification*, Prentice–Hall, Englewood Cliffs, NJ, 1994.

[28] Przekop, A., Azzouz, M. S., Guo, X., Mei, C., and Azrar, L., "Multimode Large Amplitude Vibration of Shallow Shells Considering In-Plane Inertia," 44th AIAA/ASME/ASCE/AHS Structures, Structural Dynamics, and Materials Conferences, AIAA Paper 2003-1772, Norfolk, VA, April 2003.

[29] Przekop, A., and Rizzi, S. A., "Dynamic Snap-Through Response of Thin-Walled Structures by a Reduced-Order Method," *AIAA Journal*, Vol. 45, No. 10, 2007, pp. 2510–2519. doi:10.2514/1.26351

[30] Przekop, A., and Rizzi, S. A., "Nonlinear Reduced Order Finite Element Analysis of Structures with Shallow Curvature," *AIAA Journal*, Vol. 44, No. 8, 2006, pp. 1767–1778. doi:10.2514/1.18868

[31] Kobayashi, Y., and Leissa, A. W., "Large Amplitude Free Vibration of Thick Shallow Shells Supported by Shear Diaphragms," *Journal of Nonlinear Mechanics*, Vol. 30, No. 1, 1995, pp. 35–49.

R. Ohayon
Associate Editor